Links between energy dissipation and wear mechanisms in solid epoxy/epoxy sliding contact

Olga Smerdova, Denis Mazuyer, Juliette Cayer-Barrioz

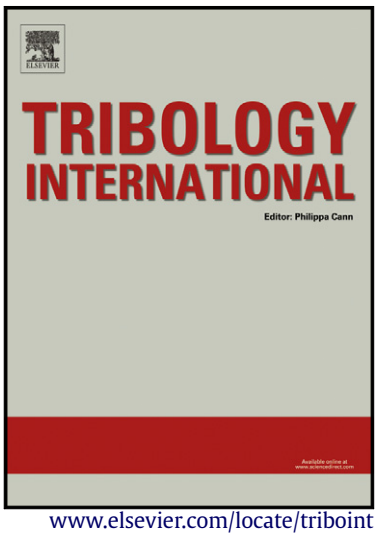

www.elsevier.com/locate/triboint

Links between energy dissipation and wear mechanisms in solid epoxy/epoxy sliding contact

Olga Smerdova, Denis Mazuyer, Juliette Cayer-Barrioz

PII: S0301-679X(14)00141-8
DOI: http://dx.doi.org/10.1016/j.triboint.2014.04.009
Reference: JTRI3299

To appear in: *Tribology International*

Received date: 14 February 2014
Revised date: 9 April 2014
Accepted date: 12 April 2014

Cite this article as: Olga Smerdova, Denis Mazuyer, Juliette Cayer-Barrioz, Links between energy dissipation and wear mechanisms in solid epoxy/epoxy sliding contact, *Tribology International,* http://dx.doi.org/10.1016/j.triboint.2014.04.009

Links between energy dissipation and wear mechanisms in solid epoxy/epoxy sliding contact

Olga Smerdova[*1], Denis Mazuyer, Juliette Cayer-Barrioz

Laboratoire de Tribologie et Dynamique des Systèmes, CNRS UMR 5513, Ecole Centrale de Lyon, 36 Avenue Guy de Collongue, 69134 Ecully Cedex, France

Corresponding author*: olga.smerdova@eng.cam.ac.uk, +44(0) 1223 7 48525.

[1] Present address: Department of Engineering, University of Cambridge, Cambridge CB2 1PZ, United Kingdom

Abstract

This paper covers wear and energy dissipation of solid epoxy induced by alternative rubbing between two samples of identical thermosetting polymer. Varying normal load, sliding velocity and sliding distance, the authors were able to define and discuss wear and friction laws and associated energy dissipation. Moreover, traces of several wear mechanisms were distinguished on the worn surfaces and associated with applied conditions. Observed under higher velocity, polymer softening and local state transition were explained by surface temperature estimate and confirmed by infra-red spectroscopy measurements. To conclude this study, all observed phenomena are classified into two wear scenarios depending on sliding velocity.

Keywords

Wear; Polymer; Sliding friction; Energy dissipation

1. Introduction

Since many years, tribologists have attempted to predict wear of different tribological systems. In spite of a large number of published experimental and theoretical investigations of this problem, a universal wear law, taking into account all parameters affecting wear, has not been proposed yet. The most famous and one of the oldest wear laws is the law of Archard [1]. Archard considered the hypothesis of plasticized contact, where the real contact area is the ratio of the normal force over the material hardness, and defined the volume of wear V_{wear} as follows:

$$V_{wear} = k_w F_N L_k / H \quad (1)$$

where k_w is the wear coefficient varying from 10^{-7} to 10^{-2} for different materials, H is the hardness of the softest surface, L_k is the relative sliding distance between the materials or kinematic length and F_N is the normal force. The low value of k_w indicates that wear is only caused from a very small proportion of asperity contacts. Furthermore, it does not depend on normal load or sliding velocity.

Nevertheless, many investigators observe similar tendencies in different frictional systems. For example, energetic approach seems to give similar answers for various wear problems [2-6]. By this approach, the dissipated energy (resp. power) is calculated from experimentally measured frictional force and sliding distance (resp. sliding velocity). It is then related to the measured wear volume in order to define the mechanisms of dissipation and wear.

For instance, Ramalho et al. [3] measured a linear wear volume–energy dissipation dependence for a couple of metals using a cross-cylinder tribometer. A similar linear

dependency was observed for fretting contacts of metals and hard coatings by Fouvry et al. [4, 5]. In their later work on fretting wear [6], the same authors were able to associate the wear mechanisms, such as plastic deformations, formation of tribologically transformed structure and stable wear regime, with the total amount of dissipated energy. Similar results were obtained in fretting wear during experiments in humid and dry atmosphere by Huq et al. [7].

Aghdam et al. [8, 9] recently proposed a method to predict friction power loss, which is a rate of energy dissipation, and wear rate from measurements of contact temperature. Moreover, they were able to correlate the average power dissipation to average contact temperature rise in sliding reciprocal friction experiments on steel alloy/brass pin-on-plate couple. As the other works above-mentioned, these authors observed a linear correlation between average wear rate and average power dissipation, too.

The linear dissipated energy-wear rate relationship was also shown to be correct for polymer/metal contacts. In the work of Colaço et al. [10], the worn volume UHMWPE increases linearly with the dissipated energy, independently of the lubricant, material used as a counterbody and of the surface finishing of both the polymer and the counterbody. To explain their results, these authors supposed a negligible contribution of contact temperature rise to the wear process. According to them, the major mechanisms responsible for energy dissipation of the polymer are viscous or plastic deformations E_{def} and generation of worn particles E_{wear}, i.e.

$$E_d = E_{def} + E_{wear} \tag{2}$$

Many experiments have been carried out to study PMMA fretting wear [11-15], in which in-situ and after test observations revealed a dependence of wear debris shape and surface damage on loading type and conditions. For instance, Geringer et al. [11] investigated a fretting wear of PMMA against a metal. These authors compared cumulated dissipated energy and C-C bond energy in order to verify if the frictional energy was dissipated in breaking these bonds. Because these values differ by a factor of 1000, they concluded that the dissipated energy is mainly used to mix and transform the third body and to expel worn particles from the contact. The good agreement between the theoretical value of the Fuller-Tabor parameter and that calculated from the experiments encouraged them to consider that only adhesion and separation load due to asperities contribute to the dissipated energy, ruling out the energy dissipation contribution:

$$E_d = E_{adh} + E_{sep} \tag{3}$$

When frictional loading is cyclic and prolonged, fatigue wear mechanism usually occurs. The proportion between fatigue wear contribution due to elastic deformations and abrasive wear contribution due to plastic deformations depends on elastic modulus and surface roughness. Dubourg et al. [16] investigated nucleation and propagation of fatigue cracks into epoxy under fretting wear conditions. Used in their experiments, epoxy material had a glass transition above 100 ^{o}C and demonstrated brittle behaviour under static fatigue and wear fretting loading. The material transparency helped them to observe that the effects of material microstructure on crack propagation mechanisms were predominated by mechanical stress-strain state undergone by the material

The present paper is aimed to bring some new insights on the wear mechanisms occurring during the friction of solid thermosetting polymer against similar polymer. The evolution of these mechanisms during sliding and increase of surface damage under different tribological conditions is a key for understanding and prediction of failure of these materials. Plane/plane configuration is chosen as it is more representative of real problems. In addition, a wide range of rather severe tribological conditions is applied in order to let the system develop the maximum of wear regimes under given geometrical and loading configuration. One can notice, that the conditions applied in this study are at the same time close to fretting, because the amplitude of sliding motion is just a triple of the contact width, and different from it, because of macroscopic size of our plane/plane system.

The energetic approach is adopted in order to link the dissipated energy to wear. Firstly, a relationship between the wear rate and dissipated energy is examined. Secondly, we relate the dissipated energy to the damaged surface area, which seems more appropriate in this case of severe wear and surface deformations. This approach allows us to discuss the energy necessary to develop surface damage by different wear mechanisms, which are detected on thoroughly examined worn surfaces after different number of sliding cycles. An additional surface analysis is performed on the worn specimens. Polymer softening and yielding observed on worn surfaces as well as sliding-induced crosslinking had suggested possible polymer state transformations, which encouraged us to estimate contact temperatures during the sliding under different conditions. Finally, all observed wear mechanisms are classified into two qualitatively different types, and a wear retrospective is proposed to evaluate the scenarios of the genesis of both types.

2. Materials & methods

2.1. Materials

All friction experiments presented in this paper are carried out on cross-linked epoxy resin HexPly® RM10.1. This epoxy resin is moulded into a large flat plate of 4±0.5 mm thickness, which is cut into rectangular samples with the approximate dimensions of 30±4 x 15±2 mm^2 for the largest specimens and 8±2 x 6±1 mm^2 for the smallest ones. The apparent sliding area of each slider is carefully measured with image treatment technique and taken into account in the following calculations. All sample surfaces are successively polished with P600, P1200, P2400 and P4000 abrasive silicon papers. The sample surface profiles are measured with Surfascan Somicronic tactile profilometer with a stylus of 2.5 µm radius tip and a step of 4 µm. The RMS roughness R_q is 0.07±0.003 µm. The average RMS waviness W_q is 0.05±0.001 µm.

The glass transition temperature of this cross-linked epoxy material is 68.8±0.2 ˚C as measured by several tests of Differential Scanning Calorimetry with heating rate of 10°C/min. Nanoindentation tests are carried out on the CSM Ultra Nanoindentation Tester with Berkovitch indenter tip under ambient environmental conditions. The penetration velocity of loading and unloading for these static indentation tests is 10 mN/min. A pause of 20 seconds is made after total loading for all indentations. These measurements are treated by the Oliver and Pharr method [17] using the value of epoxy Poisson's ratio of 0.4. Values of elastic modulus of 4.5±0.1 GPa and of hardness of 256.7±8 MPa of the epoxy material are obtained. The physical characteristics given by the supplier as well as surface mechanical properties measured with nanoindentation technique on polished samples are given in Table 1.

2.2. Experimental setup and tribological conditions

This tribological study is carried out on a linear tribometer developed in LTDS and whose principle is detailed in [18]. In this paper, the contact configuration on the tribometer is schematized in Fig. 1. A sinusoidal reciprocating motion between two flat samples fixed in stationary and moving parts of the tribometer is performed. Hereafter, the largest fixed sample will be called '*track*', while the small sample sliding upon the track will be referred to as '*slider*'. The normal load, tangential force, position and sliding velocity are continuously measured and recorded with 1 kHz sampling frequency as depicted in Fig. 1.

Four tribological conditions, summarized in Table 2, are applied in order to point out the effect of normal load and sliding speed on energy dissipation and wear. The sliding distance for all experiments is 10 mm. The applied sliding frequencies of 1 and 6 Hz correspond to the mean sliding velocity of 20 and 120 mm/s, or the maximal sliding velocity of 30 and 170 mm/s, respectively. The constant normal force is either 20 or 50 N, which corresponds to apparent contact pressure of 0.7 and 1.8 MPa, respectively. The test duration under each condition is varied between 10 and 1000 cycles in order to study the wear and friction evolution with the sliding distance. All the tests are carried out under ambient humidity and room temperature.

2.3. Kinematic conditions

The contact kinematics is also schematized in Fig. 1. All parameters discussed in this paper will be presented as a function of the kinematic length of one of the two antagonist samples. This value is defined as the distance seen by a surface point. It depends on the contact time and sliding velocities of the two contact bodies as following. Kinematic length L_{kM} of a point M belonging to the body A in contact with the body B is calculated as:

$$L_{kM} = t_M(V_B - V_A) \tag{4}$$

where V_A and V_B are the velocities of *A* and *B* contacting bodies. $t_M = b/V_A$ is a time of contact between point M and body B, where b is a contact width.

The kinematic length is similar for all points of the slider and equal to $L_{ks} = 2 \cdot l \cdot N_{cycle}$, where *l* is the sliding amplitude and N_{cycle} is the number of cycles that varies between 10 and 1000 cycles. However, the points of track surface are under different kinematic conditions and could be divided into three zones. The surface points of the two extreme zones, where the contact time depends on the point position on the surface, have less contact time than those of the central zone, where it is constant for all points. Therefore, the kinematic length is not similar for these three zones as shown in Fig. 1:

- at the beginning of the track ($0 \le x \le b$), $L_{kt} = x$, where b is the length of the contact and x is the position of the point of the track for which the kinematic length is calculated
- in the centre of the track ($b \le x \le l$), $L_{kt} = b$,
- at the end of the track ($l \le x \le b + l$), $L_{kt} = (b + l) - x$.

Further, we will operate with an average kinematic length $\overline{L}_{kt}$ for the track calculated by:

$$\overline{L}_{kt} = \frac{N_{cycle}}{(l+b)}\left[\int_0^b x dx + \int_b^l b dx + \int_l^{l+b}(b+l-x)dx\right] = \frac{2N_{cycle}}{(l+b)}\left[2\int_0^b x dx + \int_b^l b dx\right] \tag{5}$$

Thus, $\overline{L}_{kt}$ is given by:

$$\overline{L}_{kt} = 2 \cdot (bl) / (b+l) N_{cycle} \quad (6)$$

3. Experimental results: macroscopic wear and friction characterization

In order to study frictional dissipation and wear of epoxy/epoxy sliding system, a multi scale approach is developed. Firstly, a macroscopic approach is used. Several parameters, such as mass loss and corresponding wear rate, evolution of friction during each cycle and throughout the whole test and dissipated frictional energy are investigated within this framework. Secondly, this is followed by a detailed wear mechanism expertise based on the microscopic observations of worn surfaces after gradually increased test durations in order to identify the wear mechanisms and consecutive surface evolution.

3.1. Wear law

In order to measure the mass loss, all samples were weighed before and after each test. The mass losses of track and slider are plotted as a function of their respective kinematic lengths under four sliding conditions in Fig. 2 (a, b). In this plot and in other plots hereafter, each point represents the result of one experiment. The increase of the mass loss ΔM with the kinematic length L_k is roughly linear for all tested conditions. This linear dependency can be defined using one of the following ways

$$\Delta M = a_w L_k = W \rho L_k = W_s \rho F_N L_k \quad (7)$$

where W is the wear rate, *i.e.* volume loss per distance unity; W_s is the specific wear rate, *i.e.* wear rate per normal load unity, and ρ is the epoxy density.

The slope value a_w, i.e. the rate of wear, differs between the sliders and the tracks issued from the same experiment. While the slope of the former varies from 0.2 to 1.5 mg/m for the less and the most severe conditions respectively, the similar conditions cause a variation of a_w for the track from 0.3 to 2.2 mg/m. It is noteworthy, that *'HighVF$_N$'* conditions produce considerably higher mass loss, than other three conditions.

The observed linear dependence appears to be in agreement with Archard's empirical wear law Eq. (1) postulated for metallic surfaces under plastic deformations. In order to compare measured wear loss with the literature, the slope values, a_w, are reduced by epoxy density. Average wear coefficients, wear rates and specific wear rates of slider and track measured under each of four sliding conditions are reported in Table 3. All wear characteristics tend to increase with the severity of tribological conditions for both samples separately and for their couple. Nevertheless, it is noteworthy that the wear coefficient differs for the slider and the track, even under the same tribological conditions. This seems to indicate that both parts (slider and track) undergo different thermo-mechanical stress and therefore exhibit a distinct wear response.

An experimental study [19] performed on several frictional couples suggests that there is no significant difference between wear coefficients and rates of a couple of identical metals and the epoxy/epoxy couple presented here. However, it is important to emphasize, that although the increase of the mass loss with the kinematic length is linear, as predicted by the Archard model, the wear coefficient reported in this study depends on the normal load and the velocity arguing against the above model. This may be due to viscoelastic nature of the polymer and contact deformations that are not purely plastic as specified by Archard's hypothesis.

In order to verify this, the plasticity index ϕ was calculated for unworn epoxy surfaces using the values of hardness, elastic modulus and root mean square roughness parameter presented in Section 2.1. This analysis showed that contact deformations are plastic when the asperity radius is less than 21 µm. Mean radius of surface asperities of unworn epoxy surface determined from measured roughness profiles is equal to 10±4 µm. It is expected that local asperity radii would grow due to material transfer from one surface to another. In that case, the deformations would become elastic, dominating wear mechanism would be fatigue and the wear rate would be correlated with the rate of fatigue crack growth, instead of material hardness as by Archard's law.

3.2. Friction maps

Friction and normal forces are continuously measured during the experiment. Since the normal force remains roughly constant at either 20 or 50 N, as illustrated in Fig. 1, Coulomb friction coefficient can be calculated for each point of the track. The relative symmetry of the friction values between back and forth passes, which can also be seen from Fig. 1, makes possible to calculate an average value for each position. An example of Coulomb friction coefficients for a range of tribological conditions during an experiment of 500 cycles is presented in the form of friction maps in Fig. 3 (a-d), where sliding position and number of cycle are defined on x- and y-axes, respectively, and the friction coefficient is represented by colour.

As shown in Fig. 3 (a), friction remains absolutely stable during the experiment under low speed and normal force. An increase of the normal force to 50 N (see Fig. 3 (b)) leads to a rather low friction coefficient during the first 50 cycles while it subsequently increases to 0.7 and then remains stable until the end of experiment. Unfortunately, an increase of the

sliding velocity provoked the oscillations of the friction, as illustrated in Fig. 3 (c, d). This is due to a coupling between stick-slip motions at the interface and the mechanical response of the tribometer under high testing frequency. The frequency of these oscillations is about 156 Hz, which is close to the first natural frequency of the rig 173.3 Hz. The authors believe that these instabilities do not significantly affect the wear mechanisms produced by the sliding, because they concern both solids in a similar manner. An average value of friction coefficient calculated from the friction maps represents well these experiments because of its low variation with the experiment duration. For instance, its value stabilizes near 0.6-0.7 for *'HighV'* conditions, as seen from Fig. 3 (c). However, under the highest sliding and loading conditions, the mean value of the friction coefficient falls after 300 cycles from approximately 0.7 to 0.6. The drop of the friction at the top of all four maps (corresponding to the maximum amplitude of displacement of the slider over the track), shown by the blue colour, is probably due to parallelism imperfections between two planes, but can also illustrate formation and evacuation of the 3rd body.

The important conclusion from these friction measurements is that in spite of small variations during each pass, the average friction coefficient is roughly independent of the applied normal force and the velocity in the considered range of experimental conditions.

An explanation of this observation lies on the hypothesis of friction governed by interfacial shear τ and local contact pressure P i.e. the polymer hardness H, following [20]:

$$\tau = \tau_0 + \alpha P = \tau_0 + \alpha H \sim \alpha H \quad (8)$$

if the polymer hardness is high. The friction value is then constant and corresponds to the shear of the interfacial layer. Unfortunately, this hypothesis cannot be verified because the interfacial shear stress of the tested material is unknown.

3.3. Dissipated energy

Friction and wear processes generate frictional energy E_d, which dissipates in cracking, deformation, heating or tribochemical reactions. It is usually defined as

$$E_d = \int_0^{t_{exp}} F(t)V(t)dt \quad (9)$$

where $F(t)$ is the frictional force as a function of time, $V(t)$ is the sliding speed and t_{exp} is the total duration of the frictional experiment. Taking into account that the friction is rather stable during the experiment, as seen from the friction maps Fig. 3, the frictional force can be considered as $F(t)_{av} = \mu_{av} F_N$. According, to Eq. (9), the dissipated energy is found to be proportional to the kinematic length as follows

$$E_d = \sum_{i=1}^{N_{cycle}} \int_0^{1/f} F(t)V(t)dt = \mu_{av}F_N L_{ks} \quad (10)$$

The experimental results are shown in Fig. 4 as a function of the slider kinematic length. They clearly show the linear dependence of the dissipated energy on the kinematic length in agreement with Eq. (10). Pearson's linear correlation coefficients for these fittings are between 0.96 and 0.995. Their linear fitting is plotted in Fig. 4 by dashed lines with slopes of 11 N and 24 N approximately. These experimental values are close to those given by the relation $\mu_{av} F_N$, as predicted by Eq. (10).

The energetic approach presented in the introduction is adopted here to characterize the present epoxy/epoxy system. Combining Eq. (10) and Eq. (7) allows us to associate wear with frictional dissipation using the following relation:

$$E_d = \frac{\mu_{av} F_N}{a_w} \Delta M \tag{11}$$

The energy-mass diagram in Fig. 5 confirms this linear dependence between frictional dissipated energy and mass loss. Pearson's linear correlation coefficients for these fittings are 0.55, 0.93, 0.97 and 0.93 for four tribological conditions, respectively.

Eq. (11) can be written as:

$$2E_d = V_0^2 \Delta M \tag{12}$$

where $V_0 = (2\mu_{av} F_N / a_w)^{1/2}$.

This equation provides an explanation of the apparent evolution of the wear coefficients with the normal load and sliding velocity as seen in Table 2. Thus, the dissipated energy can then be interpreted as a kinetic energy. According to our experimental results, V_0 varies between 1.6 km/s and 12 km/s. These values, which are in good agreement with the slopes of the curves in Fig. 5 can be compared to that of sound propagation velocity in epoxy, V_c, which is in the range of 3 km/s [21]. As V_c corresponds to crack propagation speed in fragile rupture mode, these high values of V_0 suggests that the mass loss is due to different wear mechanisms according to tribological conditions, whether V_0 is greater than V_c or not.

Apart from providing a relevant wear law, this approach revealed a linear dependency between two independently measured macroscopic parameters, mass loss and dissipated energy.

4. Experimental results: Surface observations

The macroscopic approach links the initial and final polymer state by a quantitative characterization, without shedding light on evolution of surface state during the sliding process. The processes occurring within the plane/plane sliding contact are very complex and require very careful observations to be made. In this section, the authors attempt to retrace the history of the sliding contact, based on the micro and macro observations of the surfaces. For this purpose, the surfaces of both contact samples after rubbing 10, 100, 500 and 1000 cycles are observed through an optical microscope and analysed. First, the various types of wear mechanisms observed at microscale are listed in Section 4.1, followed by further remarks about the overall shape of worn traces in Section 4.2.

4.1. Wear mechanisms

Only few grooves are observed on the surfaces of both epoxy samples after 10 cycles under all applied conditions. Fig. 6 (a) illustrates an example of such grooves observed on a track surface after a test under *'HighF_N'* conditions. As explained by previous studies [22], the shape of worn zone borders can be associated to the ductility or brittleness of the deformed material. Therefore, the notched borders guide the assignation of the groove to the one or the other type. The transition between ductile and brittle grooves is function of normal and tangential forces, shape and size of the indenter, visco-elasto-plastic polymer properties and environmental conditions [23]. The differences in groove profile and top view of ductile and brittle types are schematized in the insets of Figs. 6 (a, b). The grooves

shown in Fig. 6 (a) exhibit side ridges, which indicates the ductility of these grooves. The grooves do not contain any trapped wear particles. Thus, we suppose that they are produced either by hard inclusions or by hard asperities of the counter-body, *i. e.* by *two-body abrasion*. The detection of two-body abrasion between two bodies of similar material is surprising at first sight. This can be explained by a difference of kinematic length between the track and the slider: the asperities of both solids do not possess similar instantaneous hardness due to thermo-mechanical softening. The larger and deeper grooves, as those produced after 100 cycles under *'HighF_N'* conditions and shown in Fig. 6 (b), are brittle.

When local asperity radii grow due to plastic deformations, the two-body abrasion mechanism is gradually changing to fatigue wear due to elastic deformations. Initially, subsurface cracks are formed due to multiple passage of conterface asperities. When these cracks reach the surface, they induce third-body formation by detaching large bulk areas. These particle then produce *three-body abrasion* in both contacting bodies.

Figs. 6 (c) and (d) present third body particles, *i.e.* worn material debris, trapped onto the track surface. These particles were created and grew during the sliding of the counter surface. They can enlarge and deepen the groove, as in Fig. 6 (c), or create a new worn zone, as in Fig. 6 (d). A smooth bottom and borders are observed in the groove indicating that the polymer has probably *yielded*.

A qualitatively-different set of worn surface phenomena that are observed on a track surface after the tests under '*HighV*' conditions is shown in Figs. 7 (a-d). The location of each observed area on the track surface is schematized in top left corner of each image. Adhesive forces grow under higher normal loads and produce higher damage to both surfaces. A material pull out, which is believed to be a consequence of high adhesion, is presented in Fig. 7 (a). The tears, observed in Fig. 7 (b) are typical for wear of elastomers under repeated

sliding friction [24]. The presence of these tears suggests that high dynamic loading has transformed the cross-linked epoxy into the *rubber state*.

Moreover, the similar nature of both contact samples and the severe tribological conditions favour *polymer transfer* between the surfaces. This process is illustrated by the adherence of compacted wear debris trapped into the track surface as in Fig. 7 (c) or the general raise of deformed worn zone borders, as it is emphasized on Fig. 7 (d).

4.2. Two groups of worn surfaces

After the tests of 100, 500 and 1000 cycles, all worn surfaces are clearly distinguishable and can be classified into two types of wear. The examples of slider and track couples, worn accordingly to these two types are given in Figs. 8 and 9. In both examples, the width of the track and slider worn surfaces are similar showing that damage occurs simultaneously on both surfaces. The slider surface is not entirely worn probably due to initial non-parallelism between the two planes. The length of the track worn zone is consistent with the central zone of maximal kinematic length, see Fig. 1. The track surface profile along the blue arrow is shown over the worn zone picture in Figs. 8, 9.

Type 1. Fig. 8 illustrates a couple of slider and track surfaces after 500 cycles under *'LowVF$_N$'* conditions. The track worn zone contains several individual macroscopic grooves forming a bigger one in the middle zone. The small quantity of matter piles up on several worn zone borders of both slider and track, but the borders are distinct. The worn surface midline is deeper than the initial surface. The worn zones of both solids are covered with the third body formed into rolls perpendicular to the sliding direction. These wear morphological characteristics are observed at low velocity (here 20 mm/s), independently of the normal load and of the number of cycles (above 100 cycles).

Type 2. Worn surfaces after the 500 cycles test under *'HighV'* conditions are shown in Fig. 9. The worn zones look fundamentally different compared to those in Fig. 8. A surface profile taken along the track worn zone reveals that its surface level is raised with respect to the initial surface as illustrated by the worn zone border in Fig. 7 (d). A part of matter is collected and trapped on the left side of the worn zone as in Fig. 7 (c), while the dark black areas correspond to deep hollows. Small tears perpendicular to the sliding direction as in Fig. 7 (b) are observed close to the middle of the track worn zone. A closer look to some track sample surfaces worn by this type reveals local colour changes to more or less yellowish or brownish colours. The slider worn surface is similar to that of the track presenting the black hollows, perpendicular tears and smooth lower border. Similarly to previous type 1, this wear morphology obtained at high velocity (here 120 mm/s) is independent of the normal load and of the number of cycles (above 100).

Due to the experimental difficulties to create absolutely parallel sliding motion between two plane samples under a constant normal load, the contact area may vary dramatically between the tests. Therefore, it is difficult to identify the conditions of transition between the several grooves wear morphology and one of the discussed wear zone types. Nevertheless, these experiments reveal that this transition occurs between 10 and 100 cycles in all cases.

5. Discussions

It seems logical to suppose that the range of polymer transformations observed under different tribological conditions is related with the dissipated frictional energy. Therefore, this section starts by linking the amount of dissipated energy with the surface area of damaged polymer. The most important mechanism of energy dissipation responsible for

polymer state change is contact heating. The authors estimate and discuss contact temperature increase, which is directly related to applied load and sliding speed. Furthermore, a possible change in mechanical properties or chemical structure in the polymer undergoing severe deformations and transformations is analysed and discussed.

5.1. Energy dissipation in increase of worn zone

Firstly, the macroscopic photos of all worn track samples are treated with ImageJ software in order to measure their worn areas. The damaged surface area A_w is estimated after this image treatment, as it is shown in Fig. 10. All visually detected types of surface damage and plastic deformation are considered to be inside the worn area.

The results of this analysis are plotted for all experiments under four tribological conditions in Fig. 11. Two regions are clearly distinguished on this diagram: the initial fast growth of the worn area with slow increase of the frictional energy until approximately A_w = 100 mm^2, followed by a faster growth of the track worn area associated with a severe increase in dissipated energy. With little difference in the slope, the initial linear region is relevant to all tested tribological conditions. The approximate rate of dissipated energy in this zone is 0.5 J/mm^2. As it was concluded from the surface observations, this region is characterized by the appearance and increase of the number of individual grooves. This region corresponds essentially to *abrasion* producing the grooves as presented in Fig. 6 (a, b).

From the second region of this diagram and our surface observations, we can conclude that when the worn area becomes larger, other wear mechanisms interfere. When the maximal damaged area is reached, the frictional process continues to dissipate energy by surface heating and possible *two* or *three-body abrasion*, *adhesive* or *fatigue wear* and

thermal transformation. If the first region is rather independent of the tribological conditions, the second region seems to indicate a strong dependence of dissipated energy rate and associated wear mechanisms on applied load and sliding speed.

5.2. Energy dissipation in heating

Relative motion between two bodies produces a work against frictional forces, which is mostly dissipated in heating of contact zone. Arising from real contact regions, the heat propagates into subsurface regions and creates temperature gradients. Unfortunately, the temperatures within the contact are very difficult to measure. However, they are of great importance because they can initiate chemical reactions or induce polymer state transformation or even degradation [25].

In order to estimate temperature gradients, contact temperatures and partition of the generated heat between two bodies, the Archard [26], Blok [27] and Jaeger [28] theory is used. A contact of a moving and a stationary body is considered. The average value of the quantity of generated frictional heat q per surface unity and time unity is given by

$$q = \frac{\mu_{av} PV}{A_r} \tag{13}$$

where A_r is the real contact area. The real contact temperature is the sum of bulk temperature θ_b, which is ambient in this case, and flash temperature rise $\Delta\theta$:

$$\theta = \theta_b + \Delta\theta \tag{14}$$

This quantity of heat is distributed between two bodies differently. Indeed, the problem is not symmetrical; the heat source is stationary for the moving slider and moving for the stationary track. Thus, the coefficient of heat partition δ is introduced.

The heat source is stationary for the slider. Therefore, its temperature gradient is calculated simply by the following equation

$$\Delta\theta_{sl} = \frac{\delta q b}{k_{sl}} \tag{15}$$

where b is the characteristic length of the contact and k_{sl} is the thermal conductivity.

For the track, the heat source is moving, and the temperature gradient depends on the ratio between the contact time for the heat source $t_c = b/V_{sl}$ and the time of the temperature propagation in the track volume $t_d = b^2/4\chi_{tr}$. In these relations, V_{sl} is the velocity of the slider, χ_{tr} is the thermal diffusivity of the track material. This ratio is introduced by the Peclet number L_P as following

$$L_P = \frac{t_d}{t_c} = \frac{V_{sl} b}{4\chi_{tr}} \tag{16}$$

The value of this non-dimensional speed criterion gives an estimate of the heat propagation profile. The temperature rise for the stationary track is given by

$$\Delta\theta_{av} = \frac{(1-\delta)q}{k_{tr}} \sqrt{\frac{\chi_{tr}\, b/2}{V_{sl}}} \tag{17}$$

Due to the equality of the track and slider surface temperature in the contact and as the two material are the same, the coefficient of partition is calculated as following

$$\delta = \frac{1}{2+\sqrt{2L_p}} \tag{18}$$

Considering the average sliding velocity V_{m1} = 20 mm/s and V_{m2} = 120 mm/s, half contact width $b/2 = 3.10^{-3}$ m and thermal properties of epoxy given in Table 1, we obtain the Peclet numbers of L_{P1} = 177 and L_{P2} = 1059. Both these numbers are very high, indicating a shallow heat propagation profile and high contact temperatures.

Coefficient of heat distribution between two solids is equal to δ_1 = 0.05 for '*LowVF*$_N$' and '*HighV*' conditions and δ_2 = 0.02 for '*HighF*$_N$' and '*HighVF*$_N$' conditions. This means that only 5 and 2 % of heat is conducted through the slider under sliding velocities V_1 and V_2, respectively. Therefore, the temperature gradient propagated into the track is much higher. On the contrary, the temperature gradient of the slider is very low, and the temperature is ambient ϑ_b in the subsurface layers of the slider.

In order to calculate the contact temperature, the knowledge of real contact area is mandatory as specified by Eq. (13). Its value is not only unknown, but varies significantly during the sliding process. At the beginning, it can be considered as a multiple asperity contact, whose area quickly grows as wear occurs. Further real area estimate is difficult due to the continuous repetitive third body formation and evacuation from the contact. For the temperature estimate, two limit values for the real contact area are considered. The upper limit is given by the apparent surface area of the slider, while for the lower limit, the Bowden and Tabor [29] formula $A_r = F_N/H$ based on the hypothesis of fully plasticized

contact is used. The real plasticized contact area under given experimental conditions is A_r = 8.8 $\times 10^{-8}$ m^2 for F_N = 20 N, and A_r = 19.5$\times 10^{-8}$ m^2 for F_N = 50 N.

The summary of relative average temperature rises for all tests under four tribological conditions as a function of the slider kinematic length is presented in Fig. 12. For both real area limits, this graph indicates two phases of temperature rise. The first cycles of fast temperature increase represent a run-in period and correspond to the sliding area increase and a third body formation. This is coherent with the initial increase of friction coefficient observed on the friction maps Fig. 3. The second region is presented by the stabilized value of the temperature rise observed under all conditions. It is noteworthy, that the temperature rise is generally higher for the faster sliding velocities by both estimate processes.

Although the real flash temperature rises are unknown due to the lack of knowledge of real contact areas, they should be somewhere between the values calculated with two limiting real area assumptions. The values of temperature rise calculated with A_{r2} are very high for all conditions. Taking into account that the glass transition temperature of epoxy is below 100 ^{o}C, such temperature rises along with the dynamical loading certainly change the polymer state to rubber-like at least locally.

In order to study epoxy thermal degradation, small epoxy chunks cut from the edge of a tested sample were heated at various temperatures. While a colour change from transparent to yellow was observed in the sample heated up to 250 ^{o}C, the heating of the epoxy up to 300 ^{o}C transformed it into dark brown. Finally, 350 ^{o}C severely degraded the epoxy sample. As it was mentioned above, slight colour changes were observed locally on the surfaces worn under high sliding speed conditions. These observations confirm that local

heating could probably reach at least 250 ^{o}C, which is considerably higher than epoxy glass transition, and transform the polymer to rubber-like state.

5.3. Change of chemical or mechanical properties in the worn zone?

The presented analysis suggests local polymer state transformation under high sliding speed. To verify if applied loading has changed the chemical organization or mechanical properties of the epoxy in the worn zone, several experimental techniques were applied by the authors.

A. Chateauminois and B.J. Briscoe [15] used the nanoindentation technique to evaluate the mechanical properties of PMMA wear debris formed during fretting wear against steel ball. These authors found almost no difference between hardness and Young modulus of the PMMA debris and those of undeformed PMMA. We believe that unlike thermoplastic PMMA, thermosetting epoxy probably modified its mechanical characteristic because of the state transformations observed above. However, the curved surface of the deformed worn zone and highly adhesive debris did not permit any trustworthy nanoindentation measurements of local surface mechanical properties.

An X-ray Photoelectron Spectroscopy (XPS) analysis was performed at several locations inside and outside the worn zone of the track sample presented in Fig. 9. This spectrometry technique gives information about the chemical environment of atoms at the surface. In our case, C_{1s}, O_{1s} and N_{1s} were investigated. This analysis performed on worn and virgin epoxy reveals that there is no significant difference between the two.

An ATR-InfraRed spectroscopic analysis was also carried out on the sample surfaces before and after sliding for various experimental conditions. The most relevant parts of the spectra of virgin epoxy sample and worn zones of track and slider samples are shown in Fig.

13. The first observation that can be made is that peak intensity is smaller for worn epoxy than that detected for virgin epoxy. This might be interpreted as a loss of motion ability of the chemical bonds due to sliding. Compared to virgin epoxy, the spectrum obtained for the slider surface under '*lowVF*$_N$' conditions after 1000 cycles displays no vibration wavelength at 784, 740 and 699 cm^{-1}. The spectrum obtained for the slider surface under '*HighF*$_N$' condition after 500 cycles is similar. In addition, a low intensity peak appears at 1647 cm^{-1}. The antagonist track surface only differs from the slider one by exhibiting a more marked peak at 1647 cm^{-1}. The loss of the vibration wavelength at 740 cm^{-1} (symmetric out-of-plane bending of the ring hydrogen), at 699 cm^{-1} (out-of-plane ring bend), and at 784 cm^{-1} (aromatic out-of-plane vibration of C-H bend), might reflect an increase in stiffness of the molecular network. This effect, accompanied by the appearance of a new peak at 1647 cm^{-1}, probably corresponding to the stretch mode of a double-C bond, under 50 N, demonstrates the influence of the experimental conditions on the wear modes. Finally, this new peak is more marked for the track surface than for the slider surface, confirming the fact that local heating is more intense and that the temperature gradient is much higher in the fixed track. Nevertheless, this analysis would require further dedicated investigation.

6. Conclusions

An analysis of wear mechanisms and associated energy dissipation in mass loss, friction and surface damage by viscoelastic, plastic deformations and state transition and chemical transformation due to heating, relevant for the sliding contact between two solid epoxy plane samples is proposed in this work. To conclude this work, a wear retrospective with two scenarios of surface damage evaluation and wear history is summarized in Fig. 14. Both scenarios start with *two-body abrasion* and then develop into one of two branches as a

number of sliding cycles increases. The following deformations are associated with the second region of diagram in Fig. 11, where various wear mechanisms interfere.

Scenario 1. The *Three-body abrasion* scenario is characterized by the presence of micro or macro grooves on the worn surfaces, see Fig. 6 (a-d) and the absence of material transfer. The majority of wear debris is evacuated from the contact, while the remaining part slides or rolls inside the moving contact and entails the deepening of wear grooves by the detachment of new wear debris from their bottom and borders. A secondary effect is the polishing of the surfaces outside the grooves by the third body rolls. A typical worn surface of track that underwent the deformations by this scenario is described as Type 1 and shown in Fig. 8. This scenario occurs under low sliding velocity for both normal loads.

Scenario 2. The *Adhesion/Thermal scenario* is characterized by two associated mechanisms: *thermal deformation* and *adhesion*. Thermal deformation is expressed in a adhesion of the compacted material to the track surface, see Fig. 7 (c), and its transfer from the slider to the track as illustrated in Fig. 9. High adhesion results in the material pull-out and in small tears perpendicular to the sliding direction, see Fig. 7 (a, b). Under higher sliding velocity, wear debris detached from the slider are not evacuated from the contact, but softened and adhere to the track surface, elevating the track surface midline. In parallel with this transfer process, the contact temperature increases as illustrated in Fig. 12. Some part of material is pulled out from the track surface, pushed by the slider to the track worn area borders and remains there as compacted wear debris. A typical example of track surface damaged according to this scenario is described as Type 2 and given in Fig. 9. This scenario is generally observed for the track and slider samples under high velocity, independently of normal load value.

The authors believe that the key difference distinguishing two scenarios is the heat-involved deformation in the surface and sub-surface layers of the polymer. This hypothesis is in agreement with the contact temperature rise and its gradient in the track samples. These calculations reveal that higher velocity causes higher contact temperature, and the largest part of this frictional heat (95-98 %) is dissipated into the track sample. Higher temperatures exceed the polymer glass temperature. This, along with the dynamic loading, causes softening of the thermosetting polymer and shifts it into rubber-like state.

Acknowledgements

The authors are very grateful to Dr Anne Rubin from ICS Strasbourg for the nanoindentation measurements, to Mr Thierry Le Mogne from LTDS for XPS measurements, to Mr Bernard Beaugiraud from LTDS for IR measurements, to Dr Alain Le Bot from LTDS and Prof. Boris Sarbaev from Bauman Moscow State Technical University for their participation to the project.

References

[1] Archard JF. Contact and rubbing of flat surfaces. Journal of Applied Physics. 1953;24:981-8.

[2] Shakhvorostov D, Pöhlmann K, Scherge M. An energetic approach to friction, wear and temperature. Wear. 2004;257:124-30.

[3] Ramalho A, Miranda JC. The relationship between wear and dissipated energy in sliding systems. Wear. 2006;260:361-7.

[4] Fouvry S, Kapsa P. An energy description of hard coating wear mechanisms. Surface and Coatings Technology. 2001;138:141-8.

[5] Fouvry S, Kapsa P, Zahouani H, Vincent L. Wear analysis in fretting of hard coatings through a dissipated energy concept. Wear. 1997;203-204:393-403.

[6] Fouvry S, Liskiewicz T, Kapsa P, Hannel S, Sauger E. An energy description of wear mechanisms and its applications to oscillating sliding contacts. Wear. 2003;255:287-98.

[7] Huq MZ, Celis JP. Expressing wear rate in sliding contacts based on dissipated energy. Wear. 2002;252:375-83.

[8] Aghdam AB, Khonsari MM. On the correlation between wear and entropy in dry sliding contact. Wear. 2011;270:781-90.

[9] Aghdam AB, Khonsari MM. Prediction of Wear in Reciprocating Dry Sliding via Dissipated Energy and Temperature Rise. Tribology Letters. 2013;50:365-78.

[10] Colaço R, Gispert MP, Serro AP, Saramago B. An energy-based model for the wear of UHMWPE. Tribology Letters. 2007;26:119-24.

[11] Geringer J, Forest B, Combrade P. Wear of poly (methyl methacrylate) against a metallic surface in dry conditions. Polymer Engineering and Science. 2007;47:633-48.

[12] Briscoe BJ, Chateauminois A, Lindley TC, Parsonage D. Fretting wear behaviour of polymethylmethacrylate under linear motions and torsional contact conditions. Tribology International. 1998;31:701-11.

[13] Krichen A, Bradai C, Chateauminois A, Kharrat M. Surface damage of poly(methylmethacrylate) under fretting loading. Wear. 1999;230:146-55.

[14] Teng J, Sato K. In situ observations of fretting wear behavior in PMMA/steel model. Materials and Design. 2004;25:471-8.

[15] Chateauminois A, Briscoe BJ. Nano-rheological properties of polymeric third bodies generated within fretting contacts. Surface and Coatings Technology. 2003;163-164:435-43.

[16] Dubourg MC, Chateauminois A, Villechaise B. In situ analysis and modeling of crack initiation and propagation within model fretting contacts using polymer materials. Tribology International. 2003;36:109-19.

[17] Oliver WC, Pharr GM. Improved technique for determining hardness and elastic modulus using load and displacement sensing indentation experiments. Journal of Materials Research. 1992;7:1564-80.

[18] Guibert M, Nauleau B et al. Conception et réalisation d'un tribometre alternatif linéaire. Tribologie et couplage multiphysiques - JIFT 2006, Lille, France.

[19] Archard JF, Hirst W. The Wear of Metals under Unlubricated Conditions. Proceedings of the Royal Society of London Series A Mathematical and Physical Sciences. 1956;236:397-410.

[20] Briscoe BJ, Tabor D. Friction and wear of polymers: the role of mechanical properties. British Polymer Journal. 1978;10:74-8.

[21] Garrett KW, Rosenberg HM. The thermal conductivity of epoxy-resin/powder composite materials. Journal of Physics D : Applied Physics. 1974;7:1247-58.

[22] Williams JA. Analytical models of scratch hardness. Tribology International. 1996;29:675-94.

[23] Guibert, M., Nauleau, B. et al.: Conception et réalisation d'un tribometre alternatif linéaire. Tribologie et couplage multiphysiques - JIFT, Lille, France 2006.

[24] Briscoe B. Wear of polymers: an essay on fundamental aspects. Tribology International. 1981;14:231-43.

[25] Kennedy FE, Tian X. The Effect of Interfacial Temperature on Friction and Wear of Thermoplastics in the Thermal Control Regime. 1994. p. 235-44.

[26] Archard JF. The temperature of rubbing surfaces. Wear. 1959;2:438-55.

[27] Blok, H. General discussion on lubrication and lubricants. Inst. Mech. Eng. London 1937;2:222-35

[28] Jaeger JC. Moving sources of heat and the temperature at sliding contacts. Proc.of the Royal Soc. NSW 1942;76:203-24

[29] Bowden FP, Tabor D. The Friction and Lubrication of Solids: Clarendon Press; 2001.

Table 1. Physical and mechanical properties of the epoxy resin

Density ρ, kg/m^3	**Thermal conductivity *k*, W/m K**	**Specific heat capacity c_p, J/kg K**	**Thermal diffusivity χ, m^2/s**	**Glass temperature, ˚C**	**Elastic modulus, GPa**	**Hardness, MPa**
1.1×10^3	0.19	1×10^3	0.17×10^{-6}	68.8 ± 0.2	4.5 ± 0.1	256.7 ± 8

Table 2. Applied tribological conditions

Conditions	'LowVF_N'	'HighV'	'HighF_N'	'High VF_N'
Normal load (F_N), N	20	20	50	50
Average apparent contact pressure (p), MPa	0.7	0.7	1.8	1.8
Sliding distance (l), mm	10	10	10	10
Frequency (f), Hz	1	6	1	6
Average sliding velocity (V_m), mm/s	20	120	20	120
Max sliding velocity (V_{max}), mm/s	30	170	30	170

Table 3. Wear volume loss characteristics

Conditions	'LowVF$_N$'	'HighV'	'HighF$_N$'	'HighVF$_N$'
Slider/Track mass loss a_w (mg/m)	0.2/0.3	0.2/0.7	0.3/0.6	1.5/2.2
Slider/Track Archard's wear coefficient, k_w (×10^{-3})	1.2/4.4	0.9/2.7	2.9/9.5	6.1/8.8
Slider/Track wear rate, W (×10^{-10} m^3/m)	0.9/3.5	1.8/5.3	2.3/7.4	11.8/17.1
Slider/Track specific wear rate, W_s (×10^{-11} m^3/Nm)	0.5/1.8	0.4/1.1	1.2/3.7	2.4/3.4

Highlights

- An experimental study on polymer/polymer asymmetric contact wear is reported;
- A range of wear mechanisms was identified for several tribological conditions;
- An energy dissipation was calculated based on friction measurements;
- The wear is related to the energy dissipation for each of applied conditions;
- Higher sliding speed cause local polymer state transition and post cross-linking.

Figure(s)

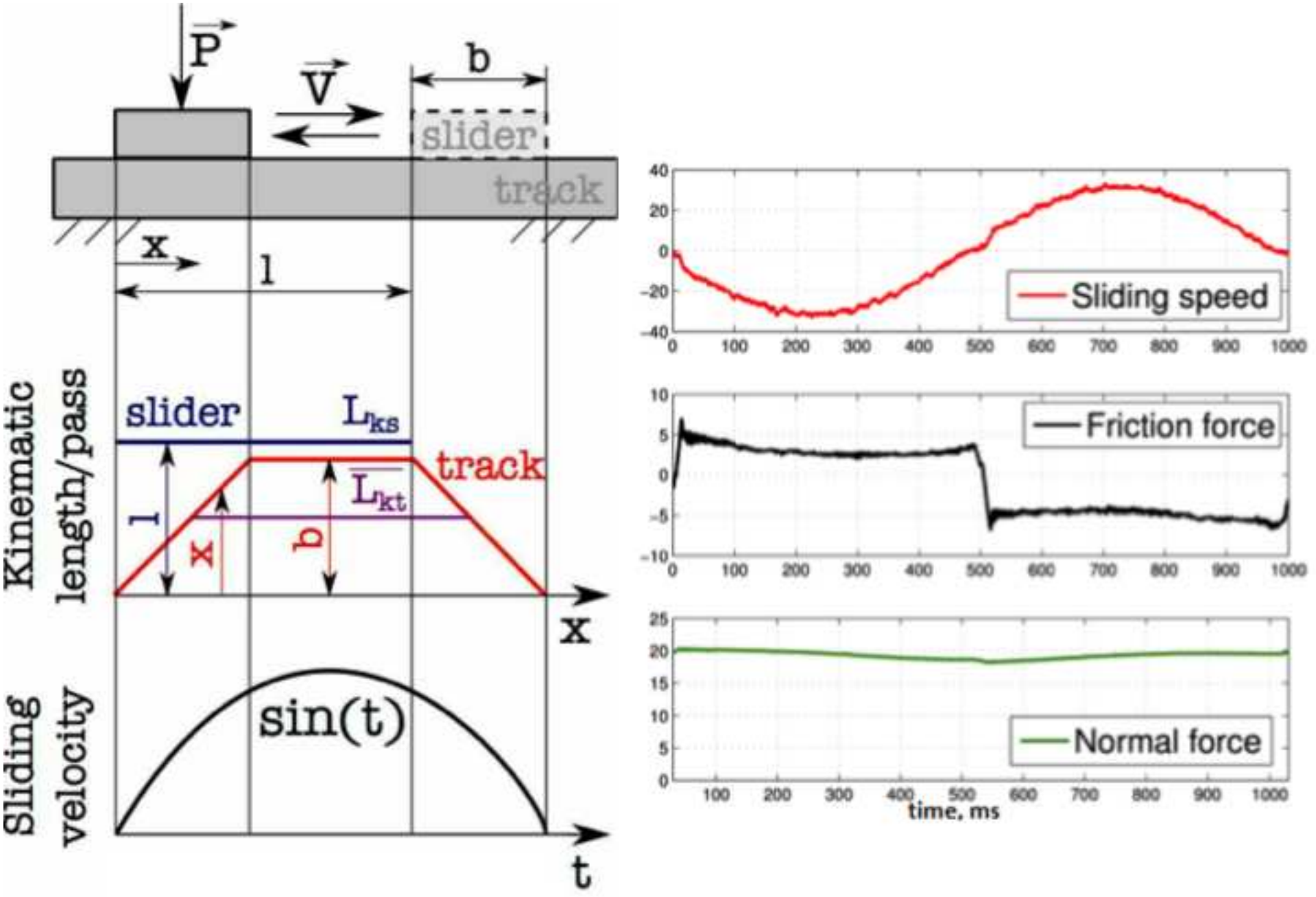

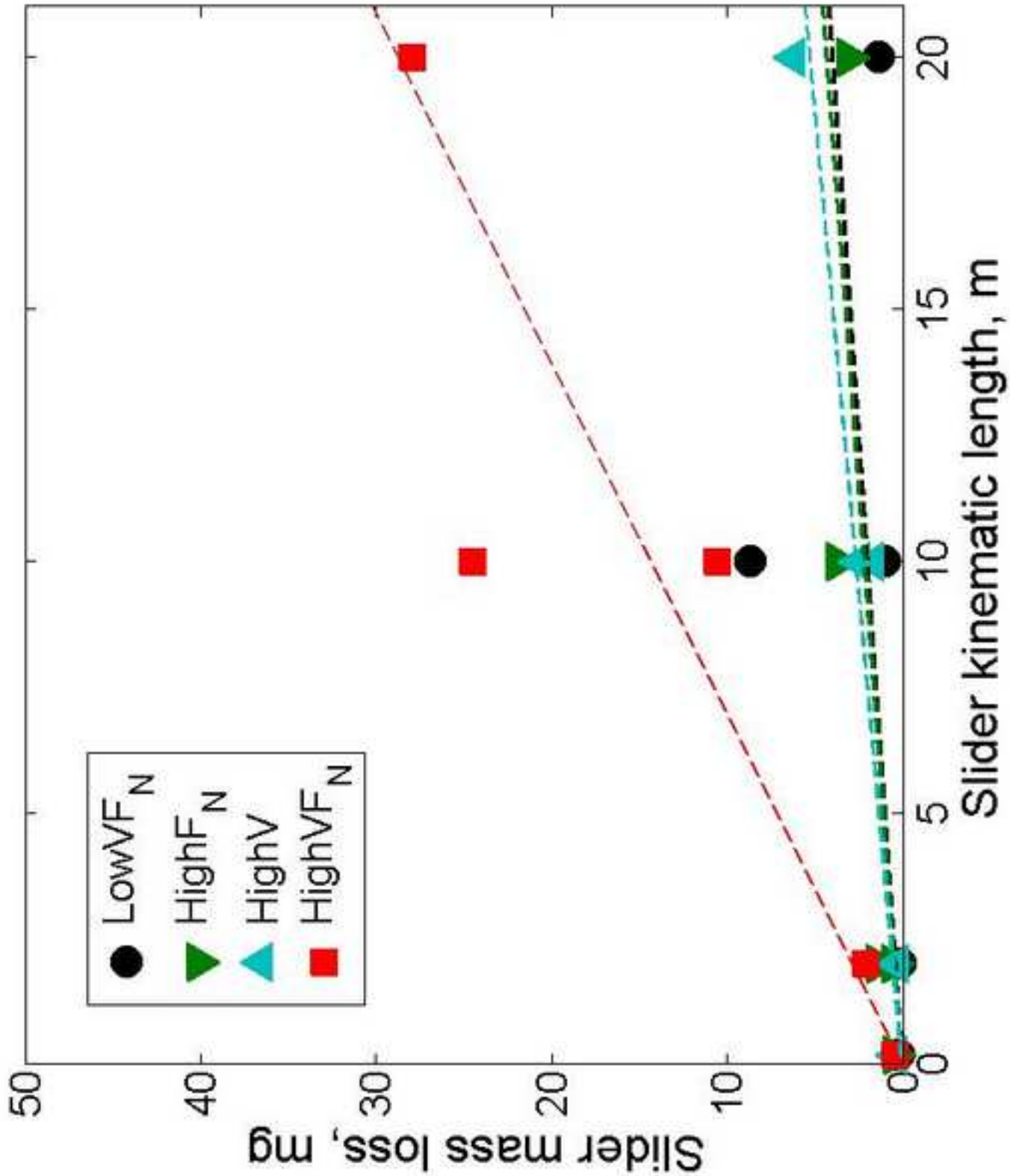
Slider mass loss, mg
Slider kinematic length, m
0
10
20
30
40
50
0
5
10
15
20
LowVF$_N$
HighF$_N$
HighV
HighVF$_N$

Figure(s)

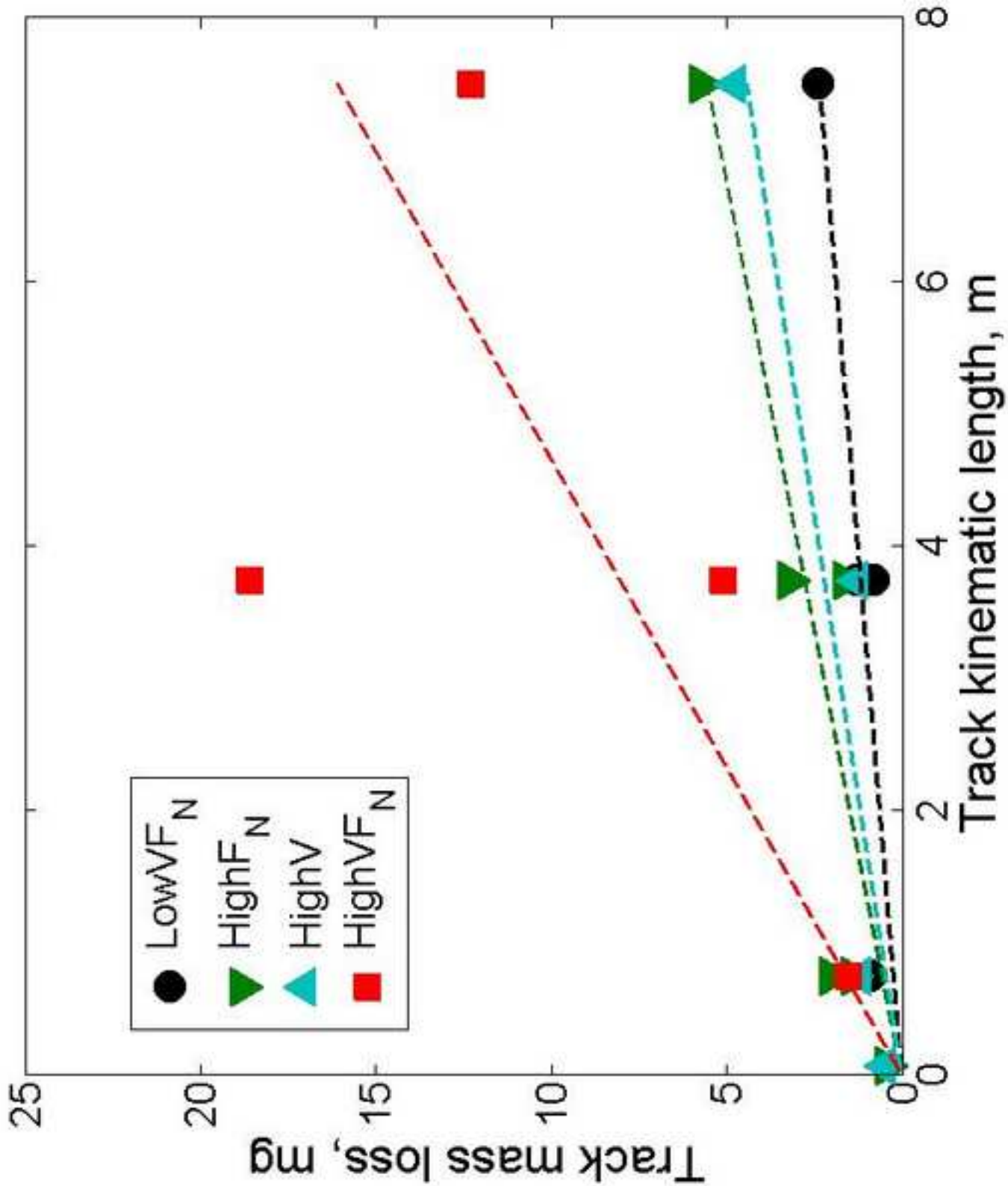
Track mass loss, mg
Track kinematic length, m
0
5
10
15
20
25
0
2
4
6
8
LowVF$_N$
HighF$_N$
HighV
HighVF$_N$

Figure(s)

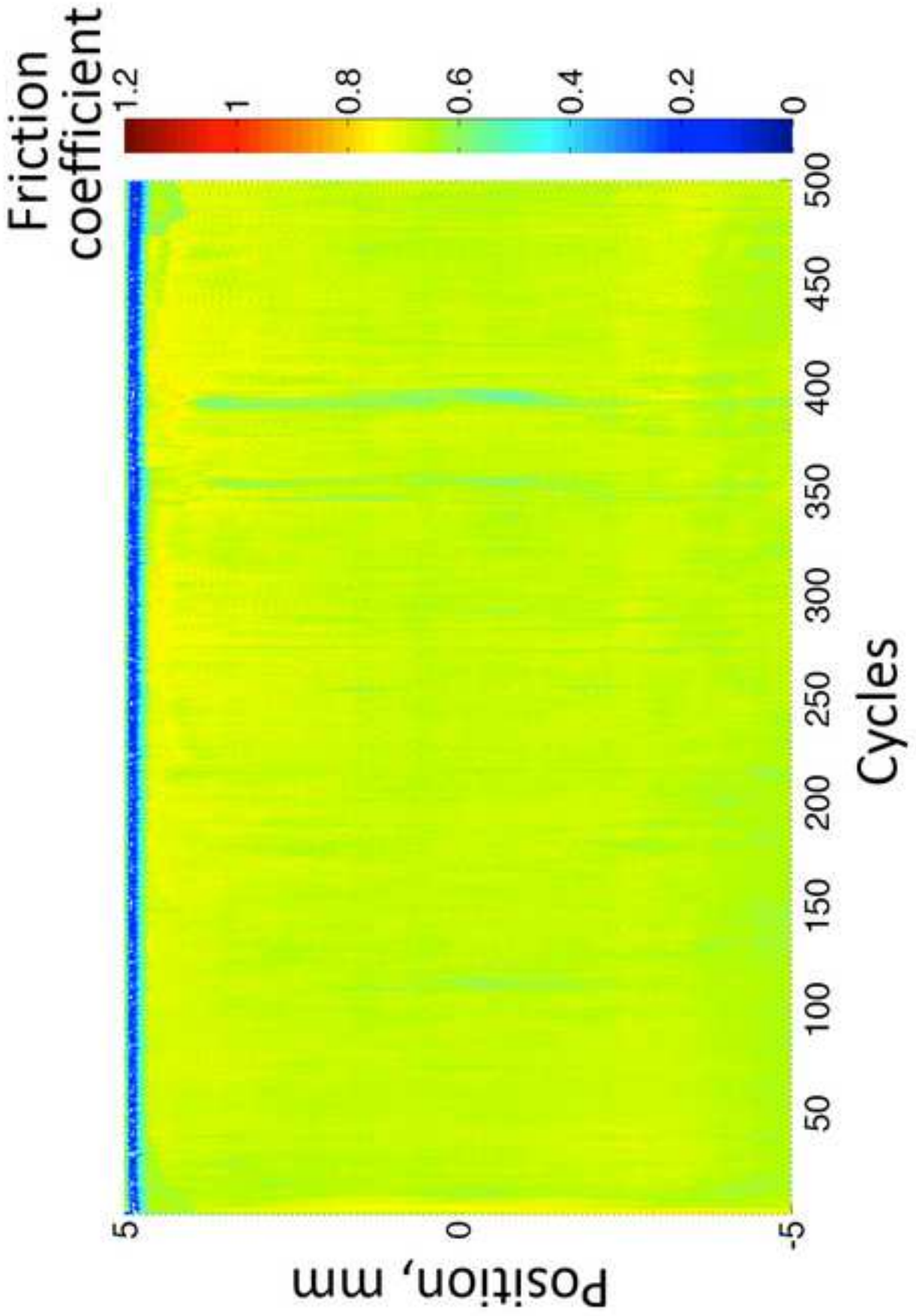

Figure(s)

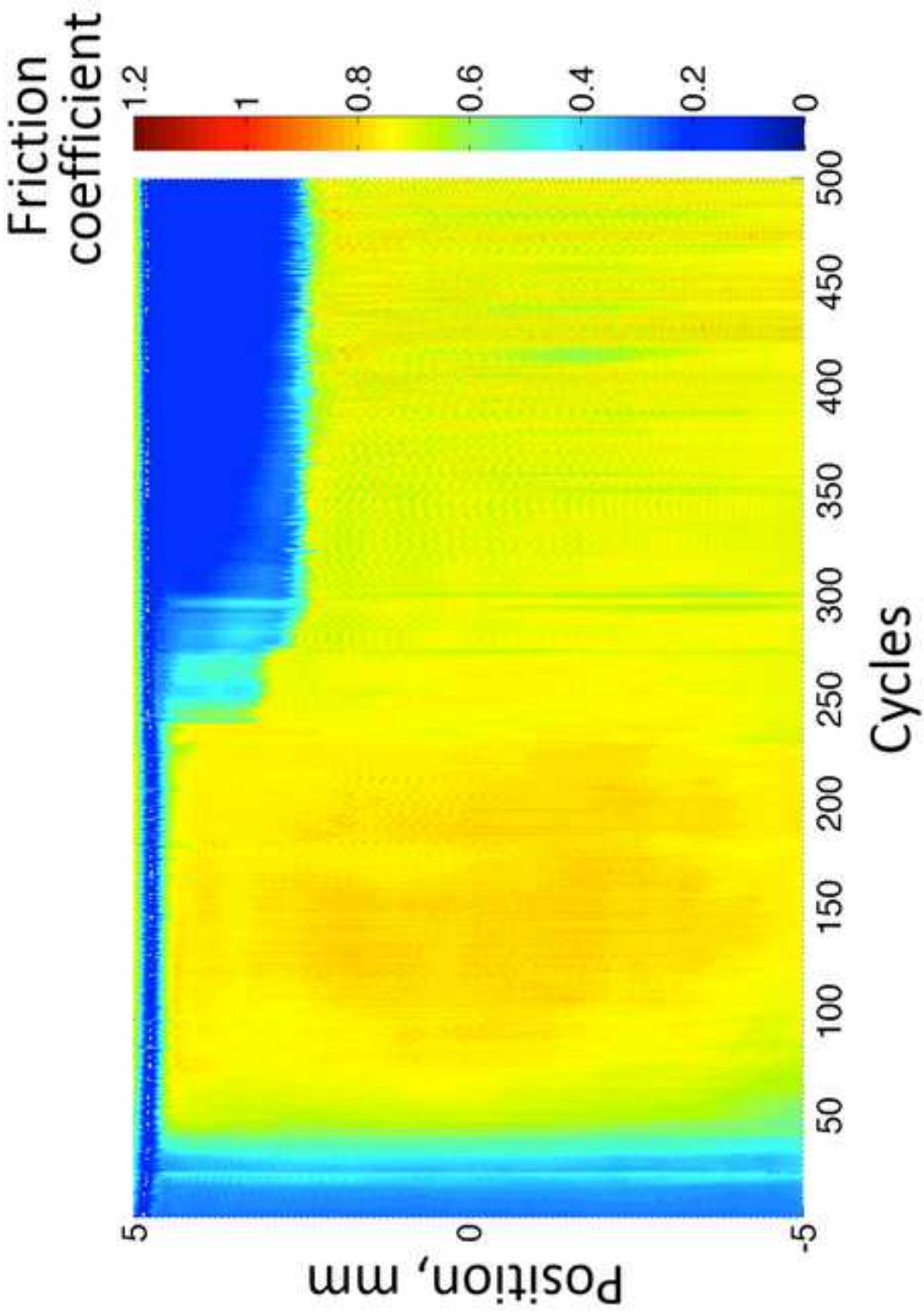

Figure(s)

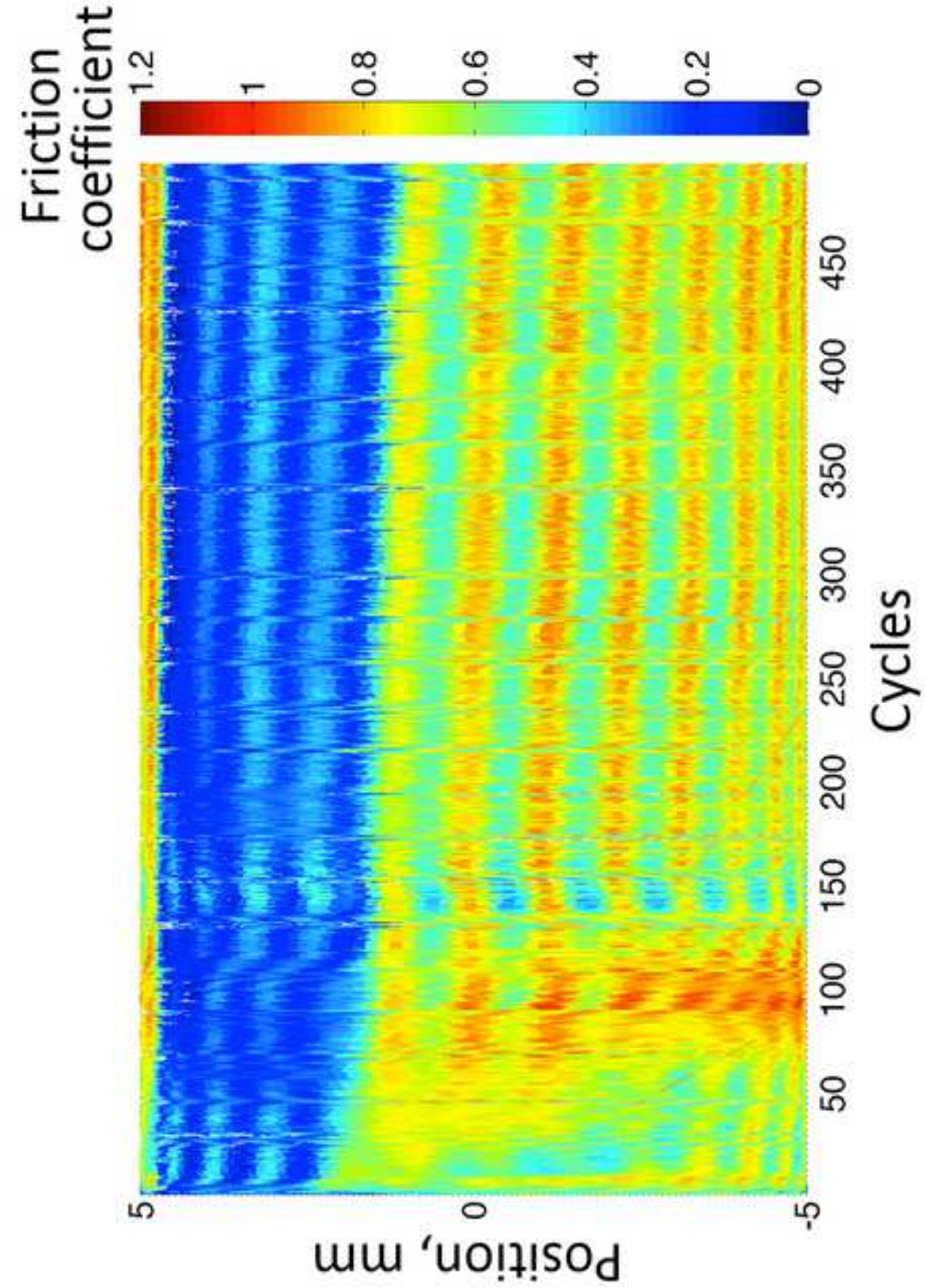

Figure(s)

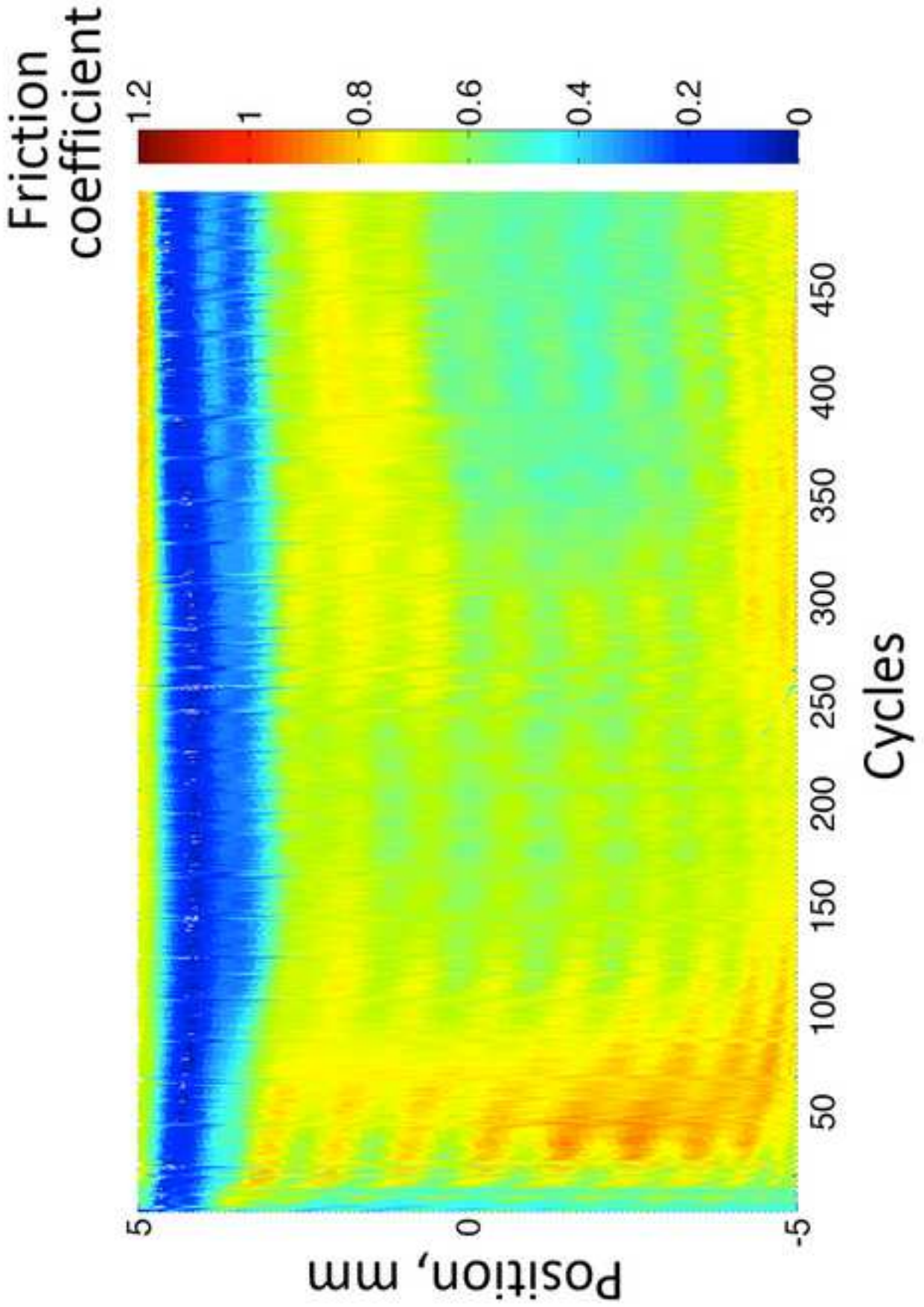

Figure(s)

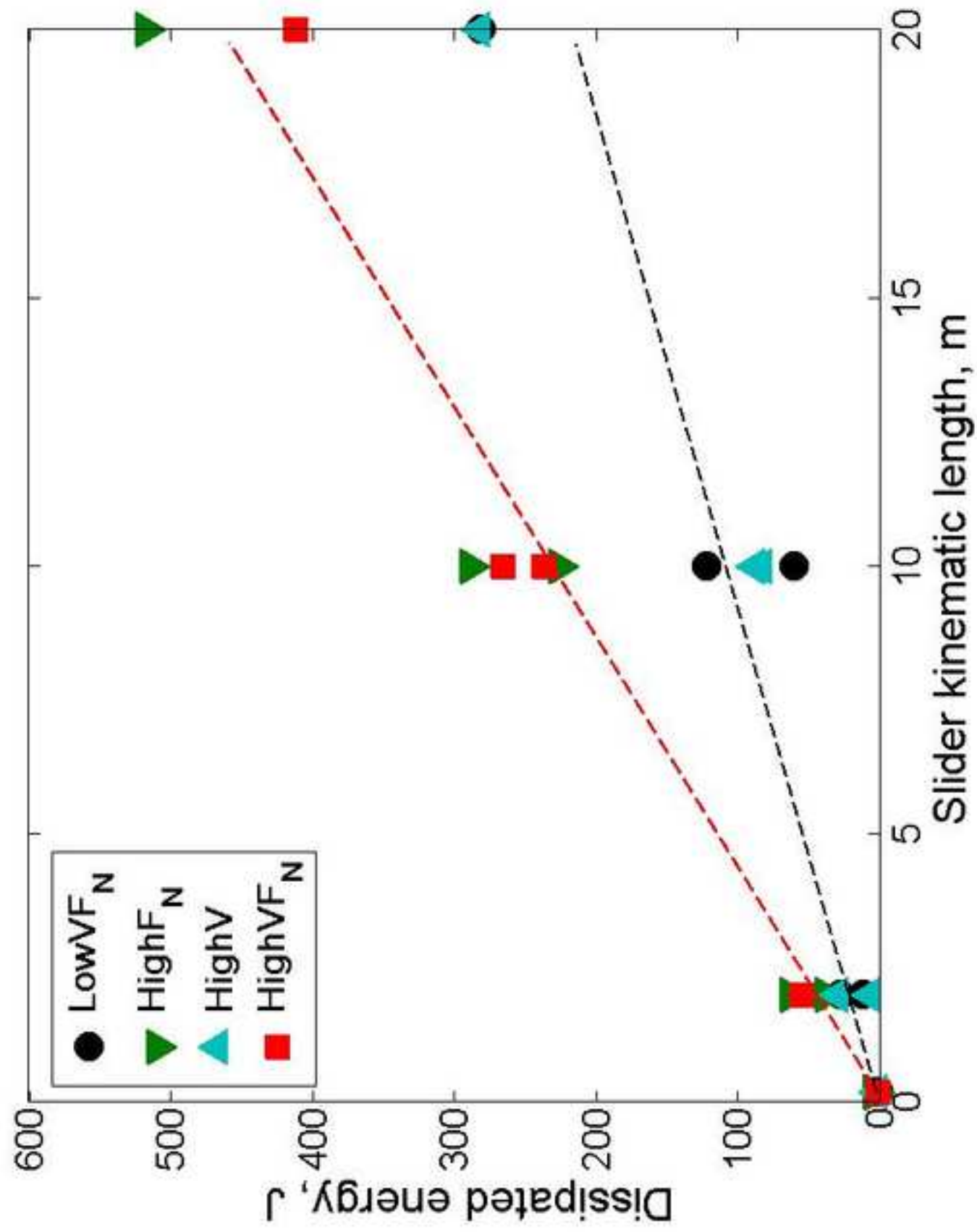

Figure(s)

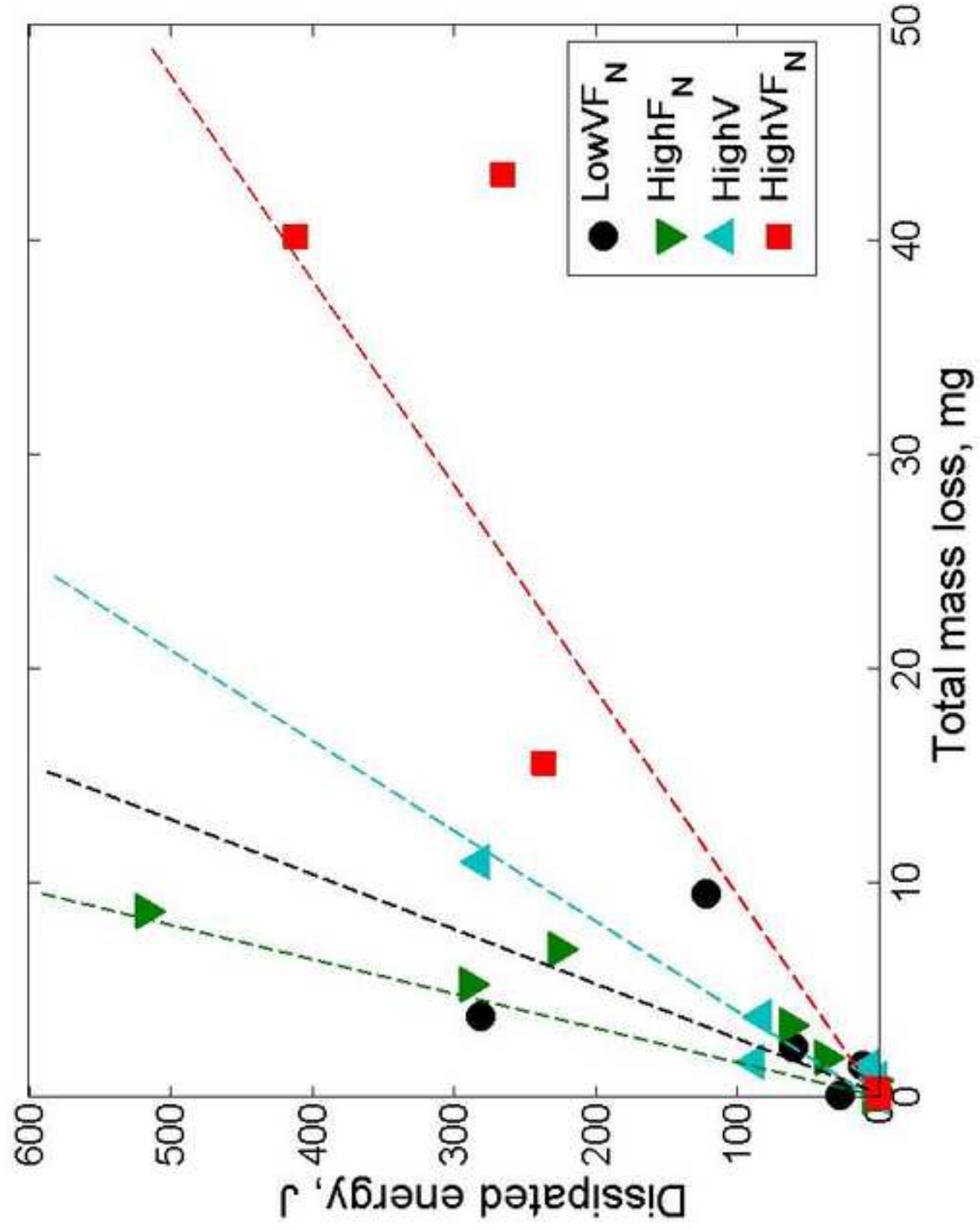
Dissipated energy, J
Total mass loss, mg
LowVF$_N$
HighF$_N$
HighV
HighVF$_N$
0
100
200
300
400
500
600
0
10
20
30
40
50

Figure(s)

Figure(s)

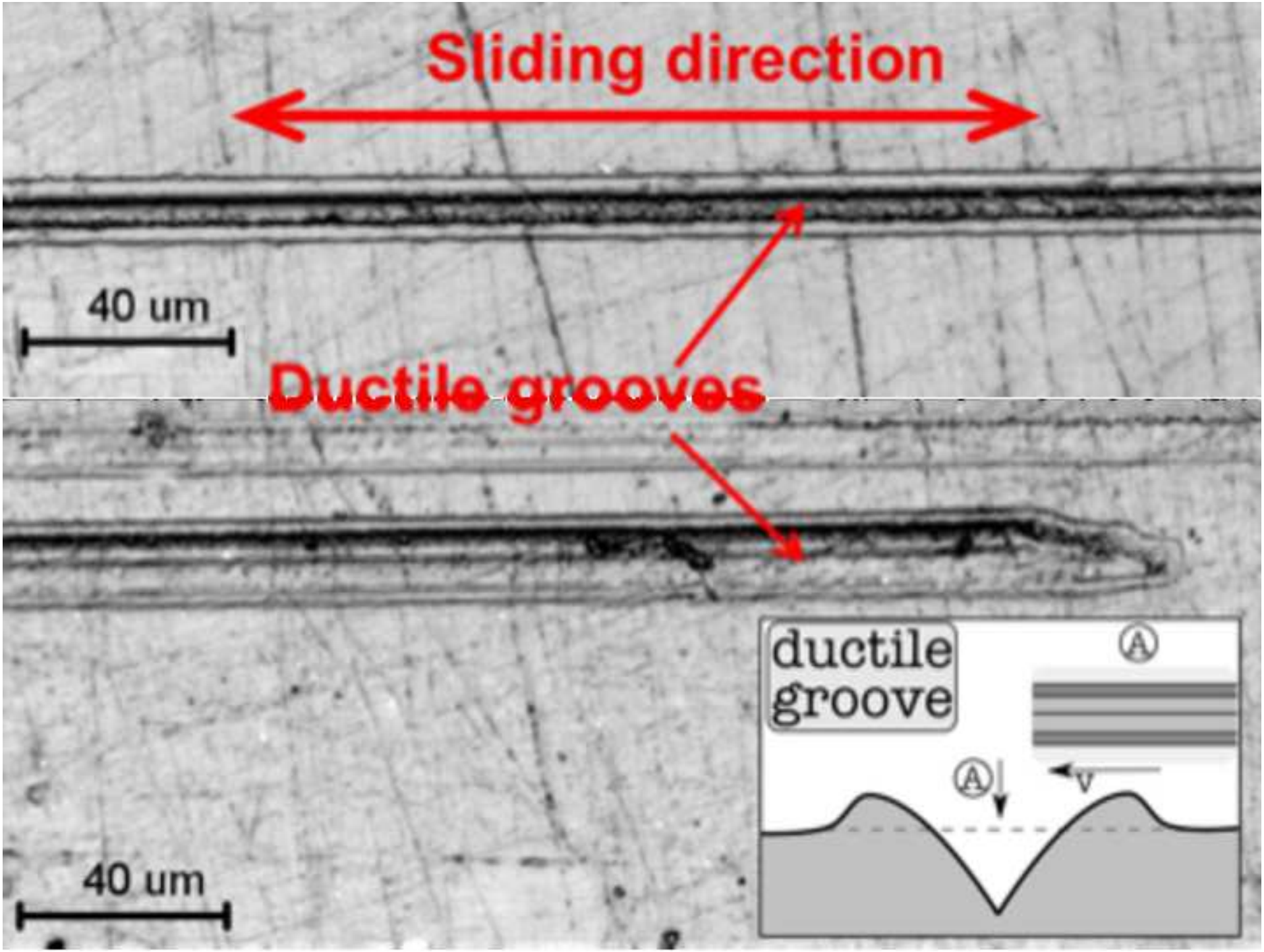

Figure(s)

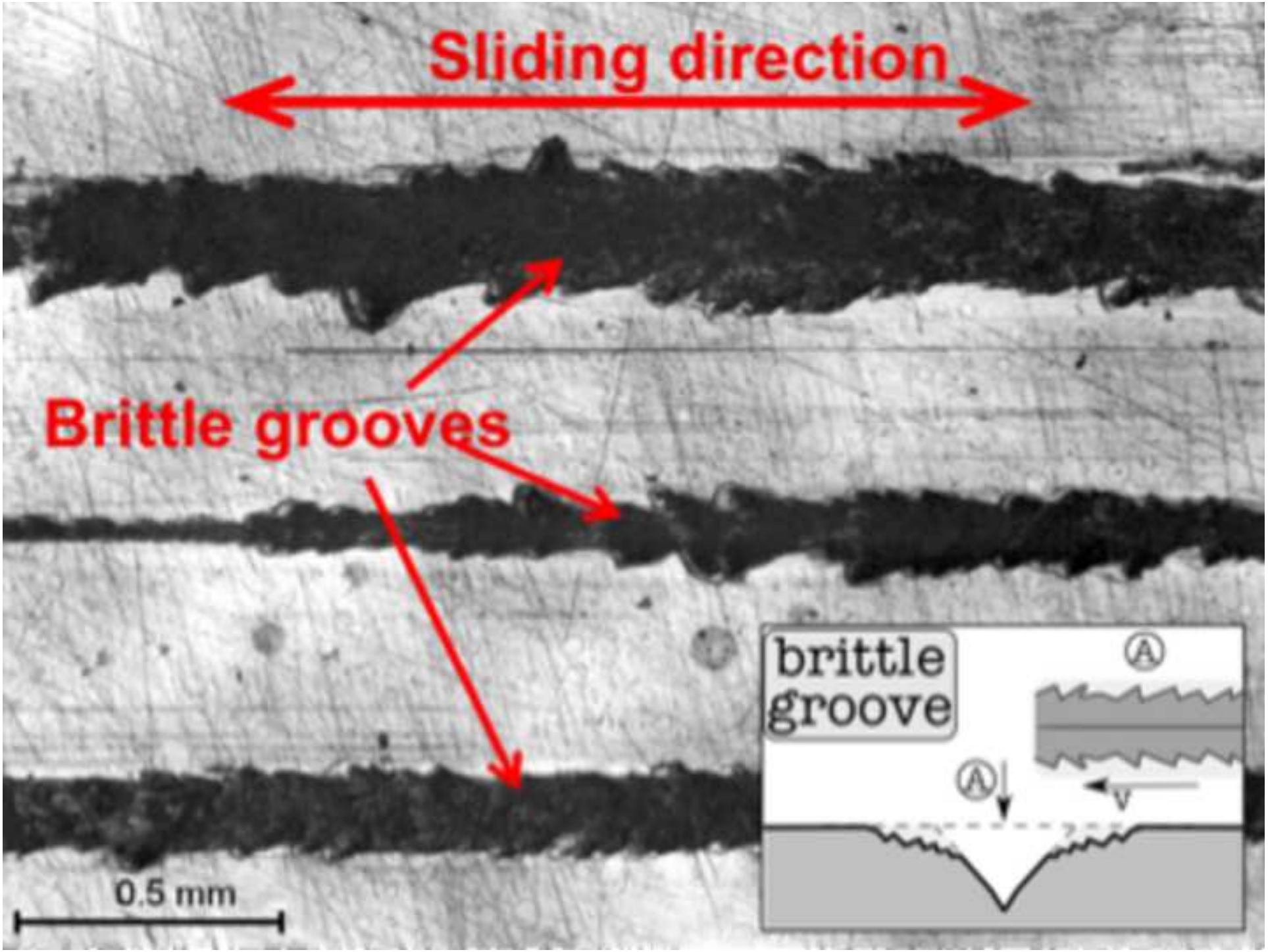

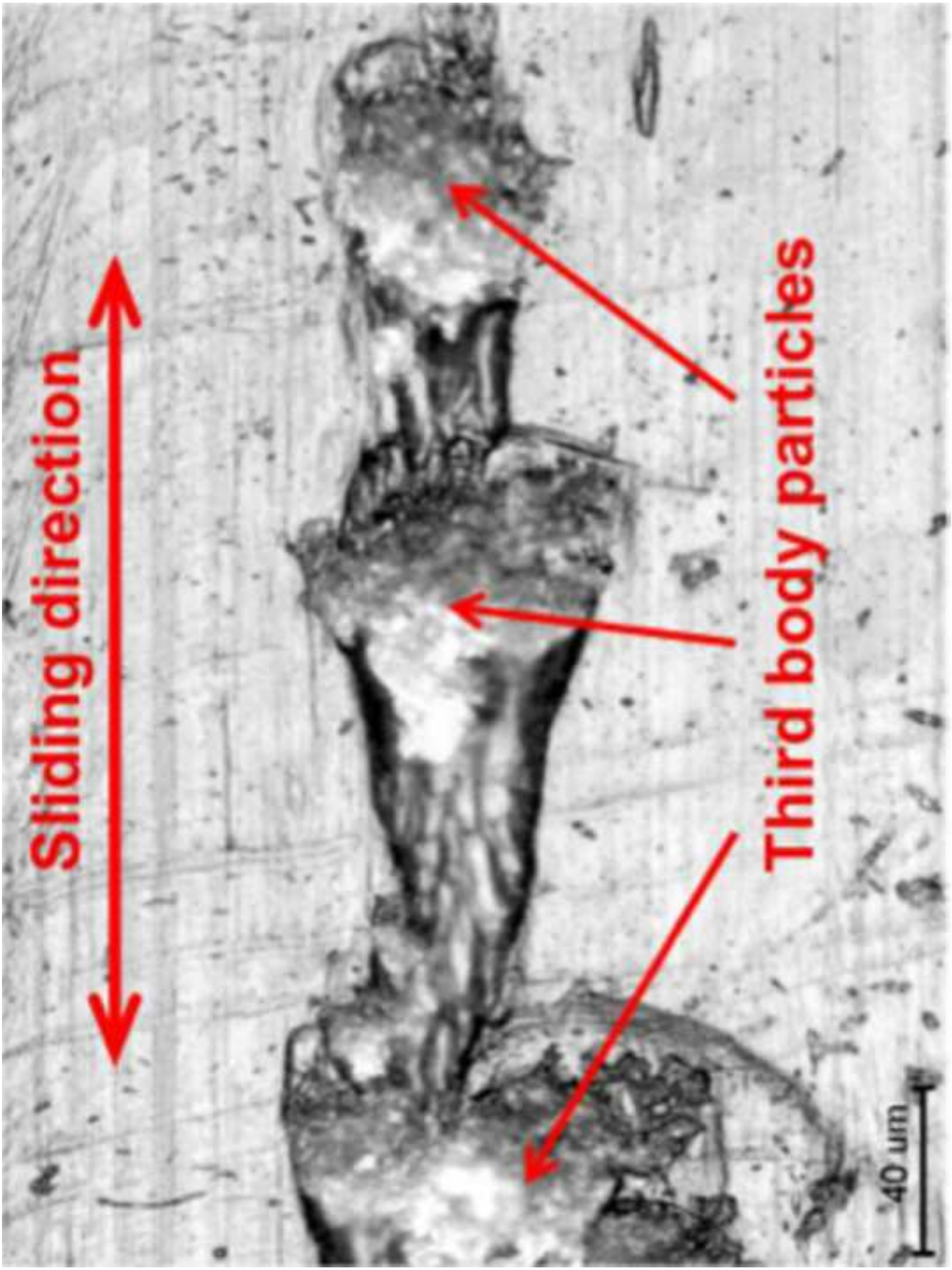

Figure(s)

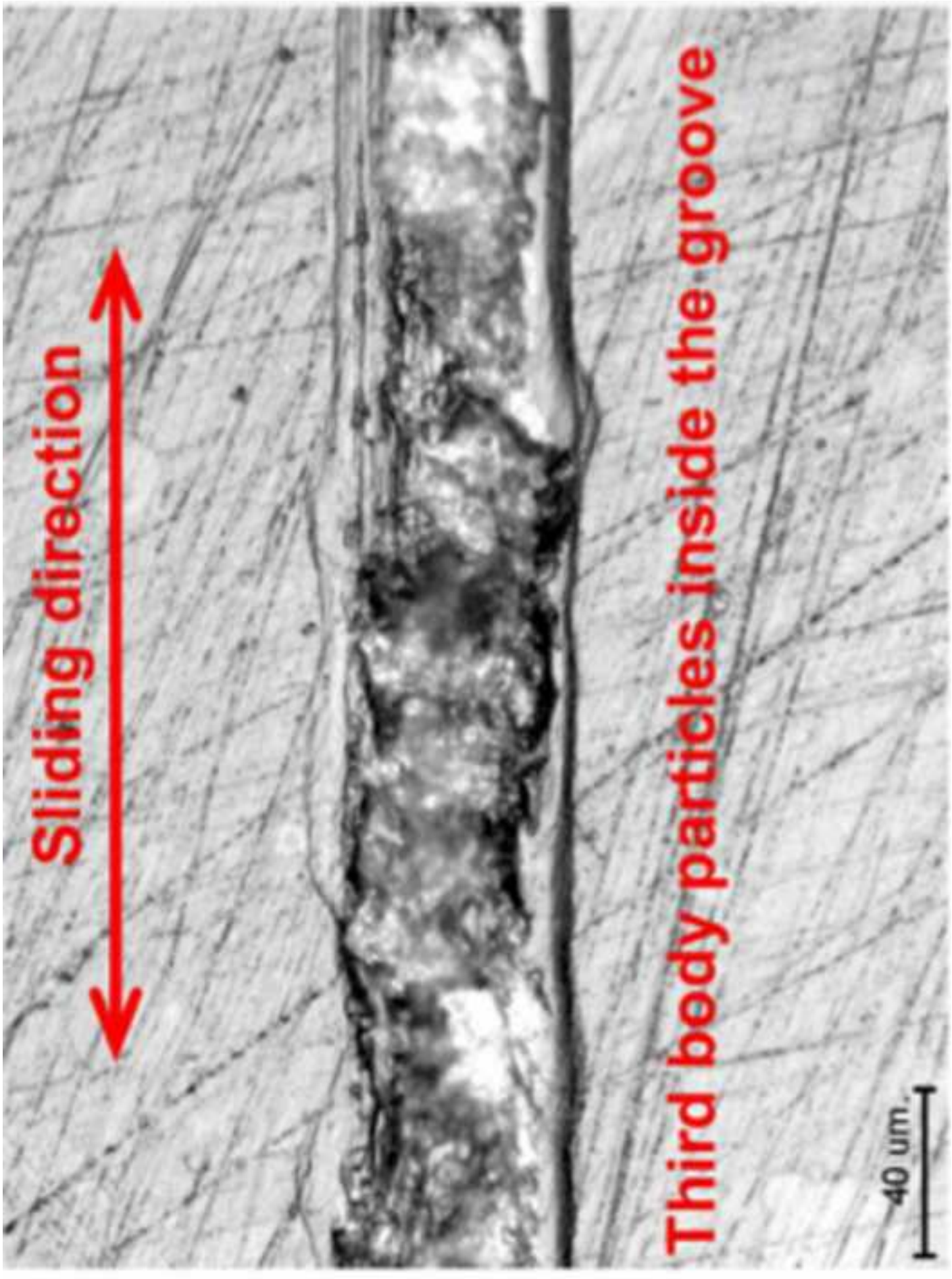
Sliding direction
Third body particles inside the groove
40 um.

Figure(s)

Figure(s)

Figure(s)

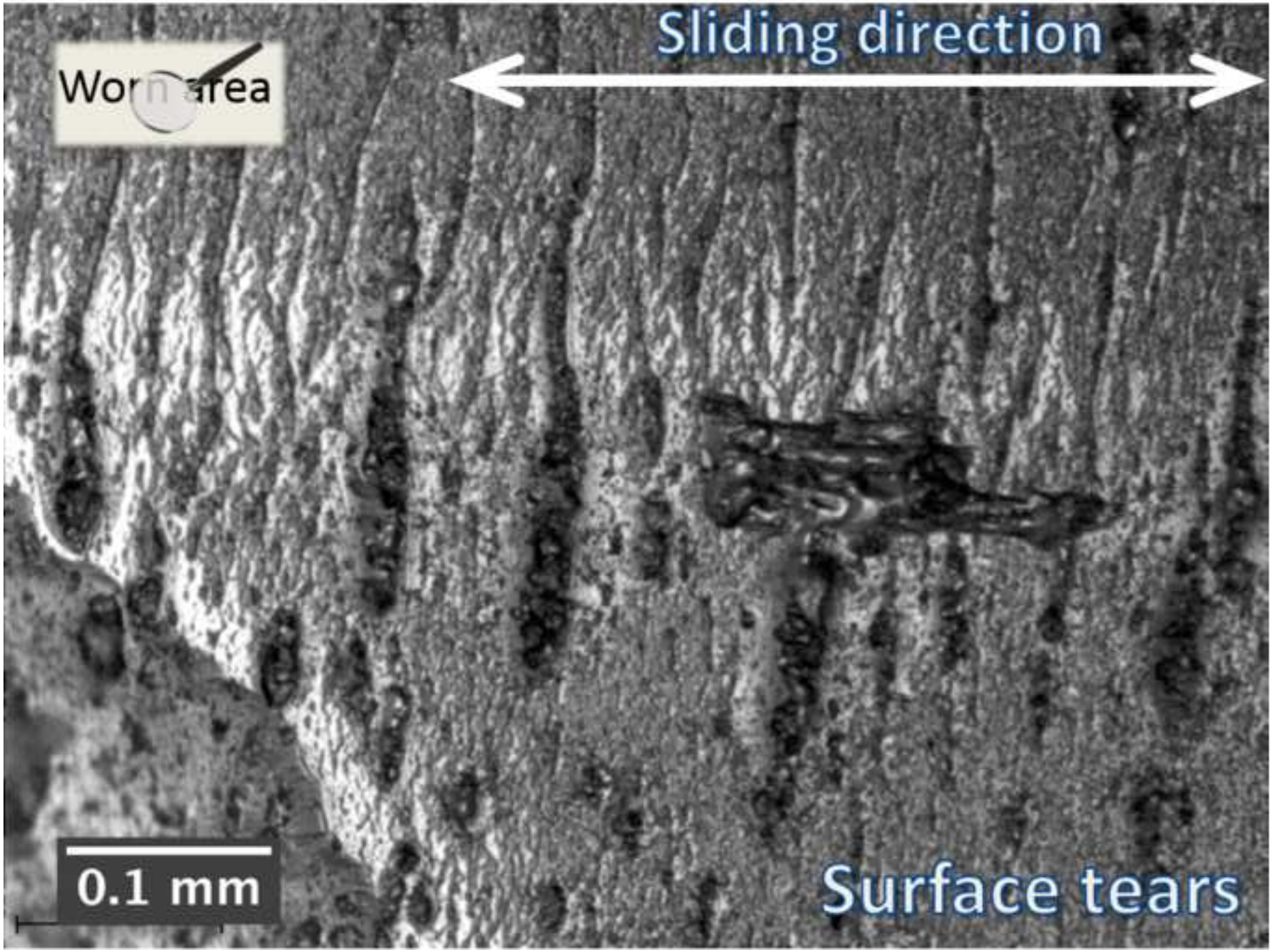

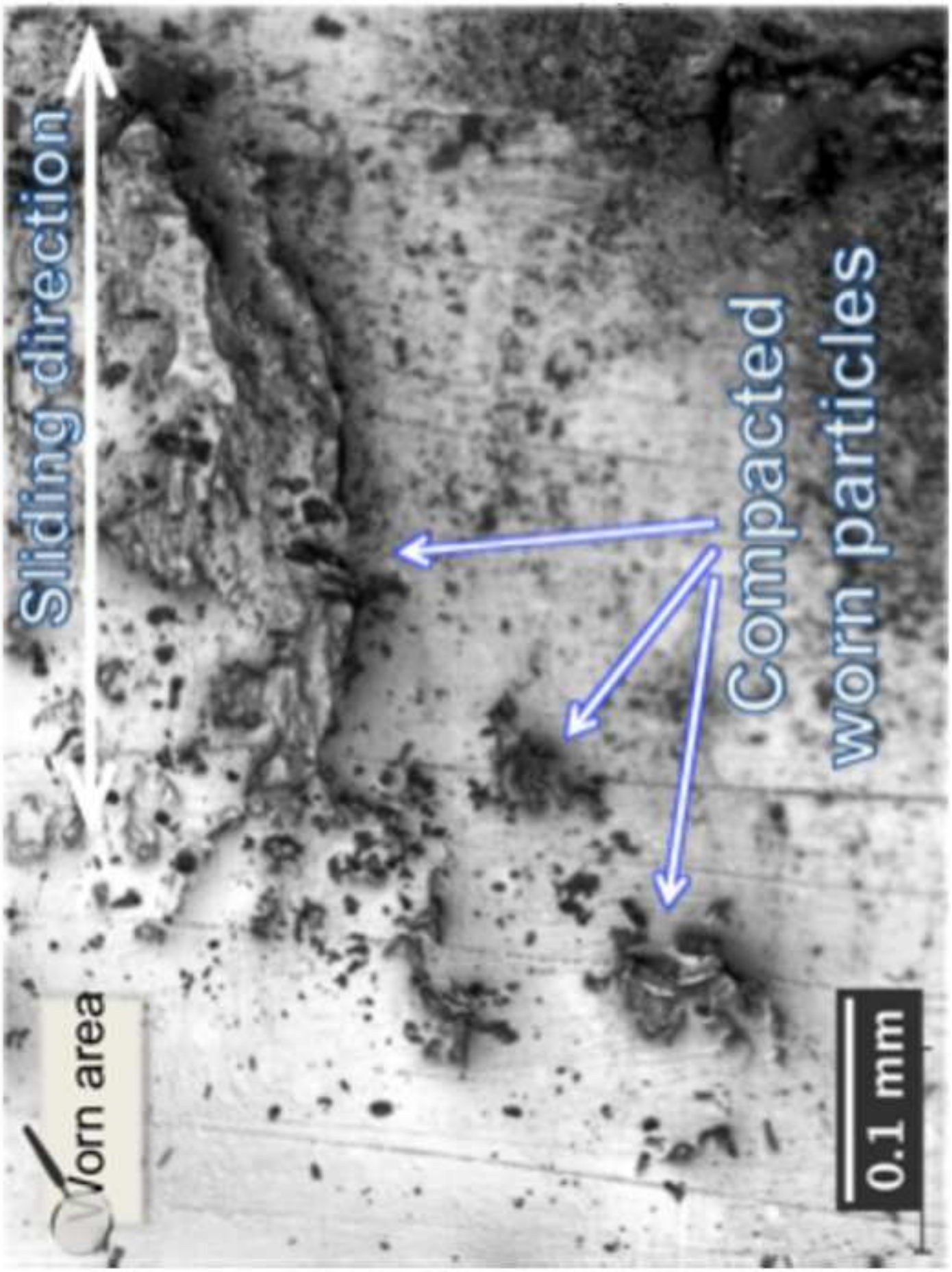
Sliding direction
Worn area
Compacted worn particles
0.1 mm

Figure(s)

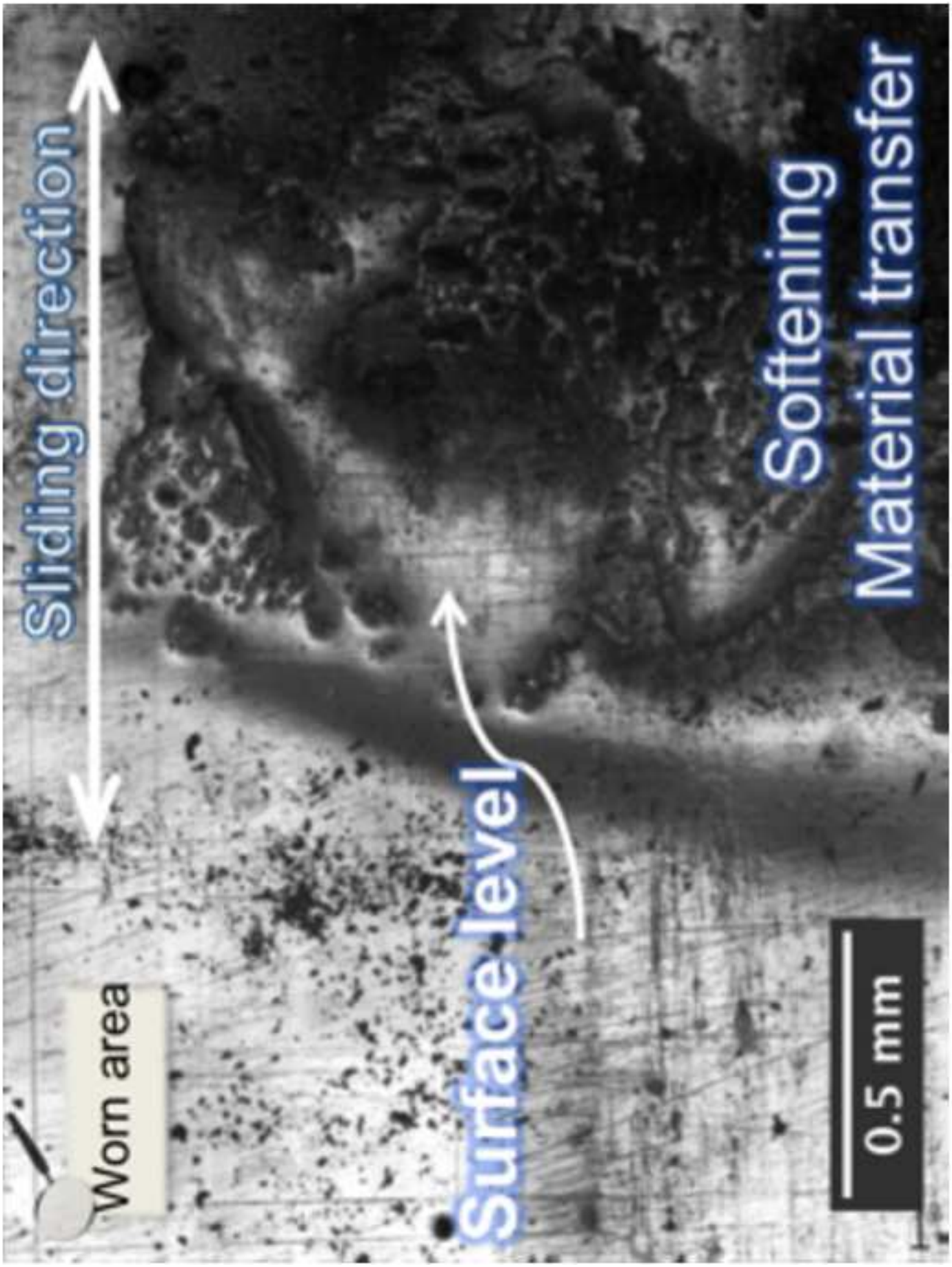
Sliding direction
Worm area
Surface level
Softening
Material transfer
0.5 mm

Figure(s)

Figure(s)

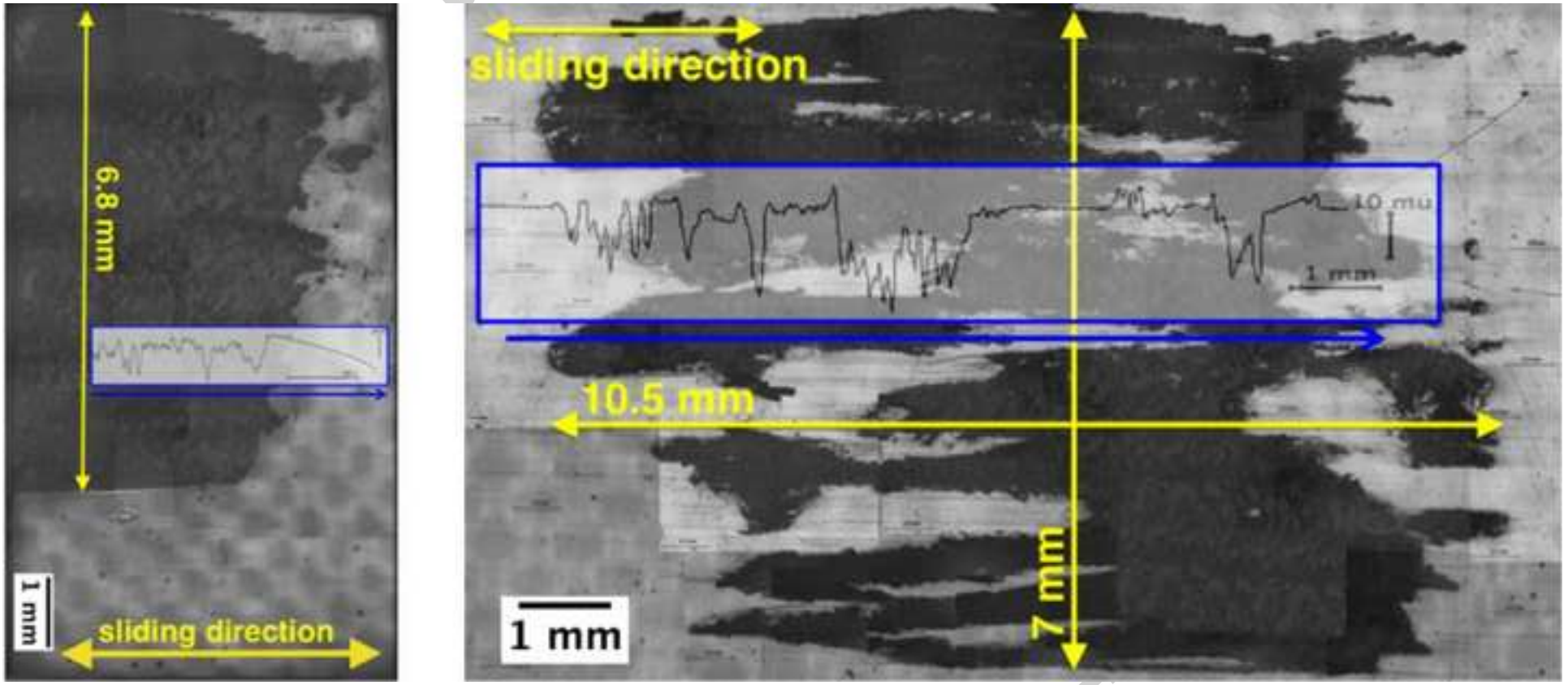

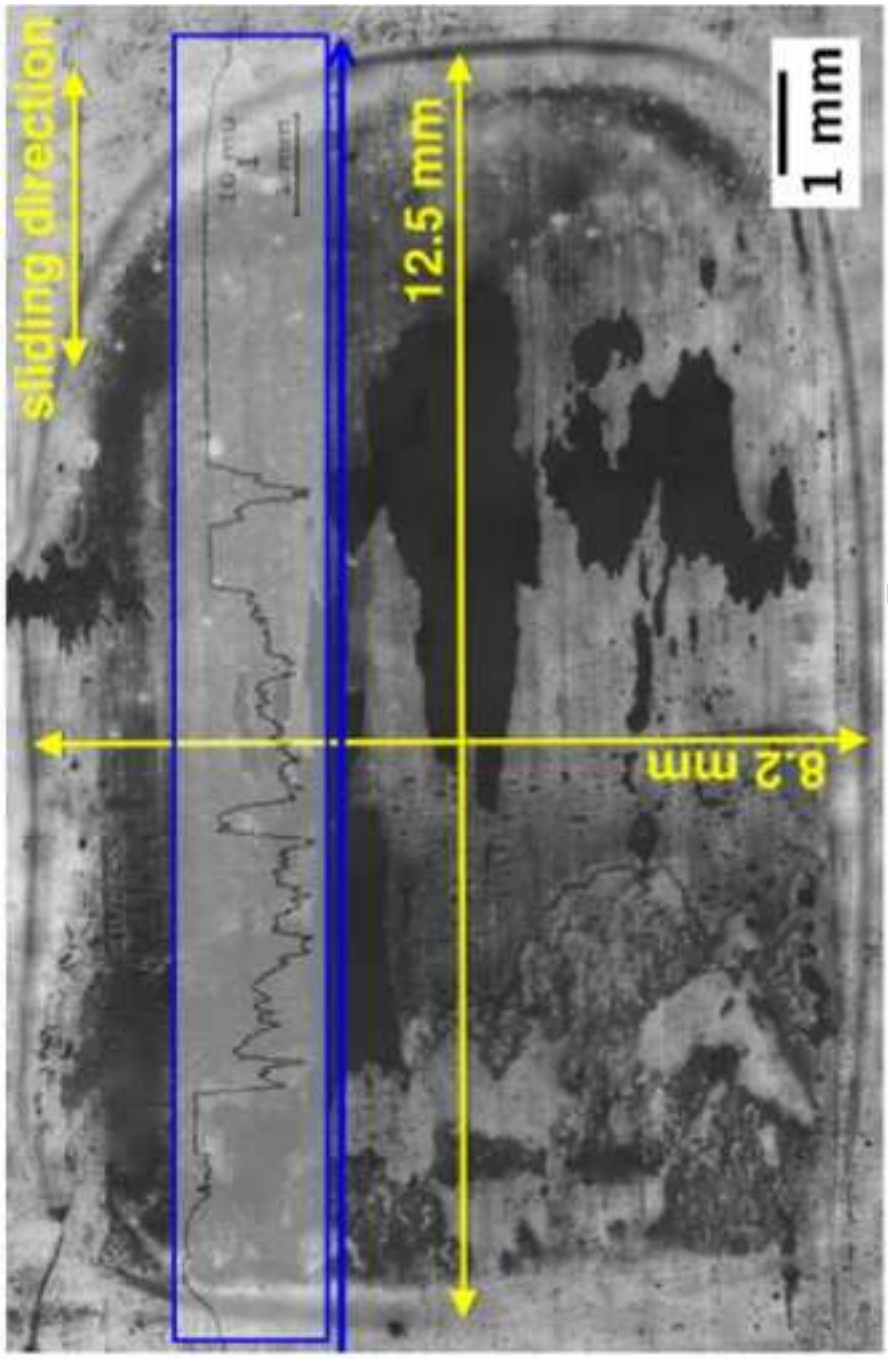
sliding direction
12.5 mm
8.2 mm
1 mm

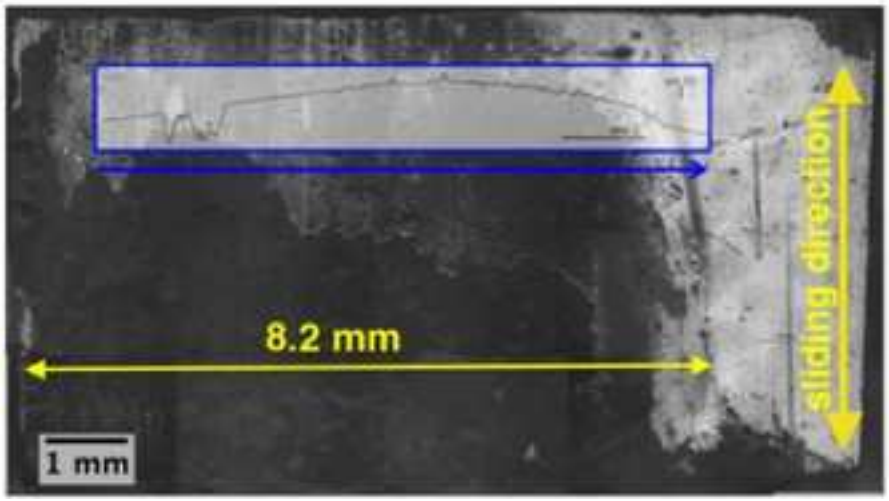
8.2 mm
sliding direction
1 mm

Figure(s)

Figure(s)

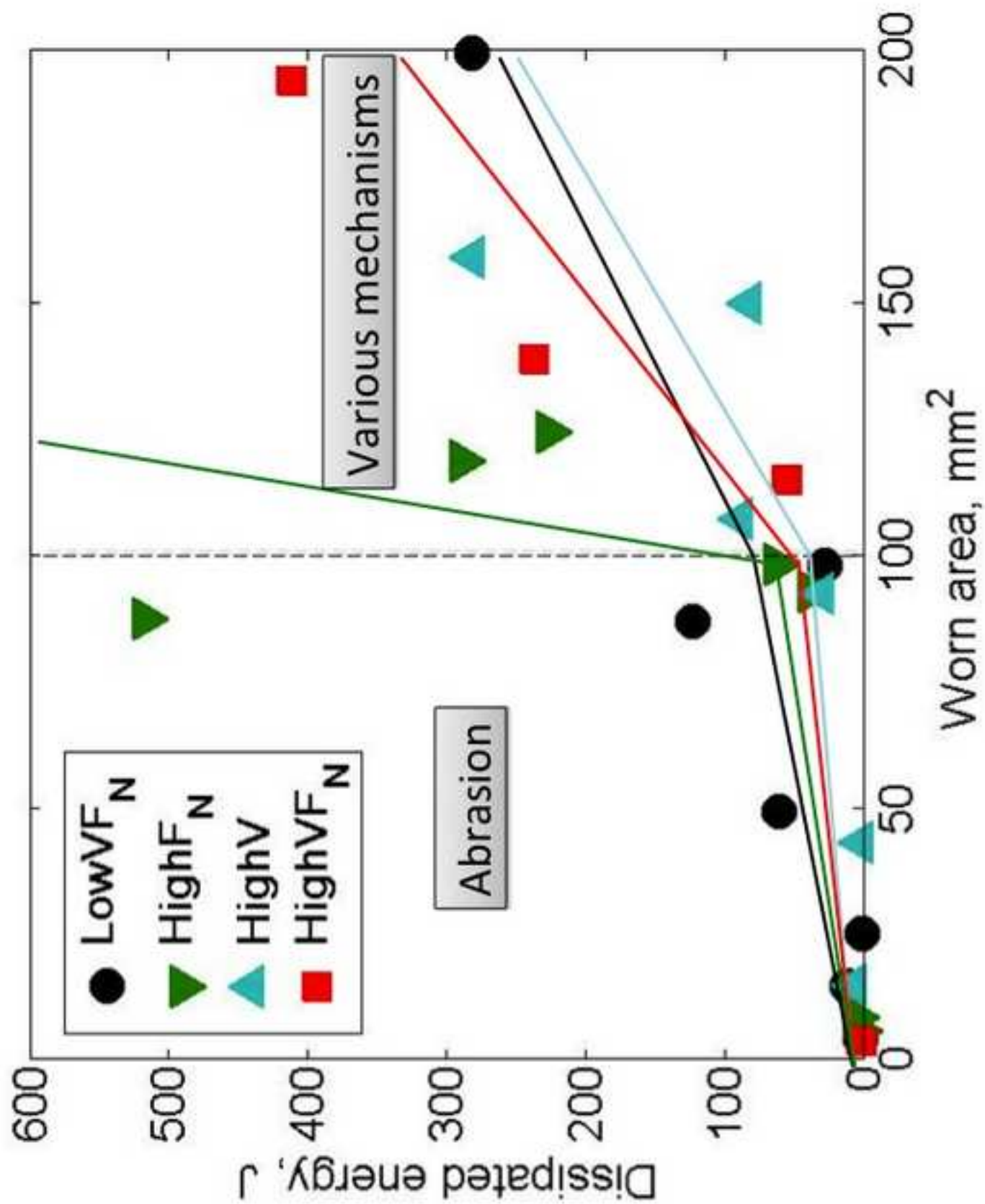
Dissipated energy, J
Worn area, mm2
0
100
200
300
400
500
600
0
50
100
150
200
Various mechanisms
Abrasion
LowVFN
HighFN
HighV
HighVFN

Figure(s)

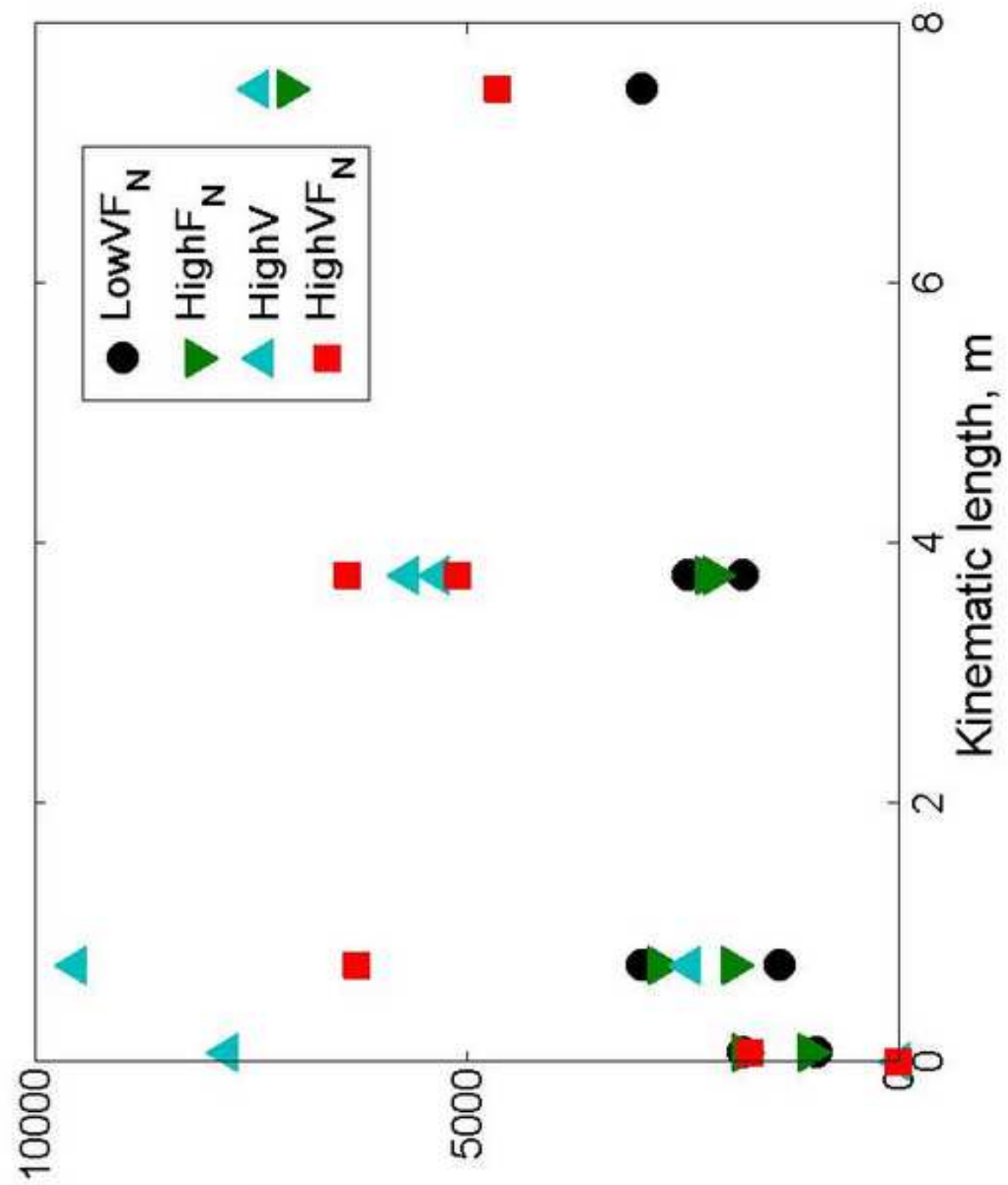
LowVF_N
HighF_N
HighV
HighVF_N
Δv Temperature based on Δ_T [°C]
Kinematic length, m
10000
5000
0
0
2
4
6
8

Figure(s)

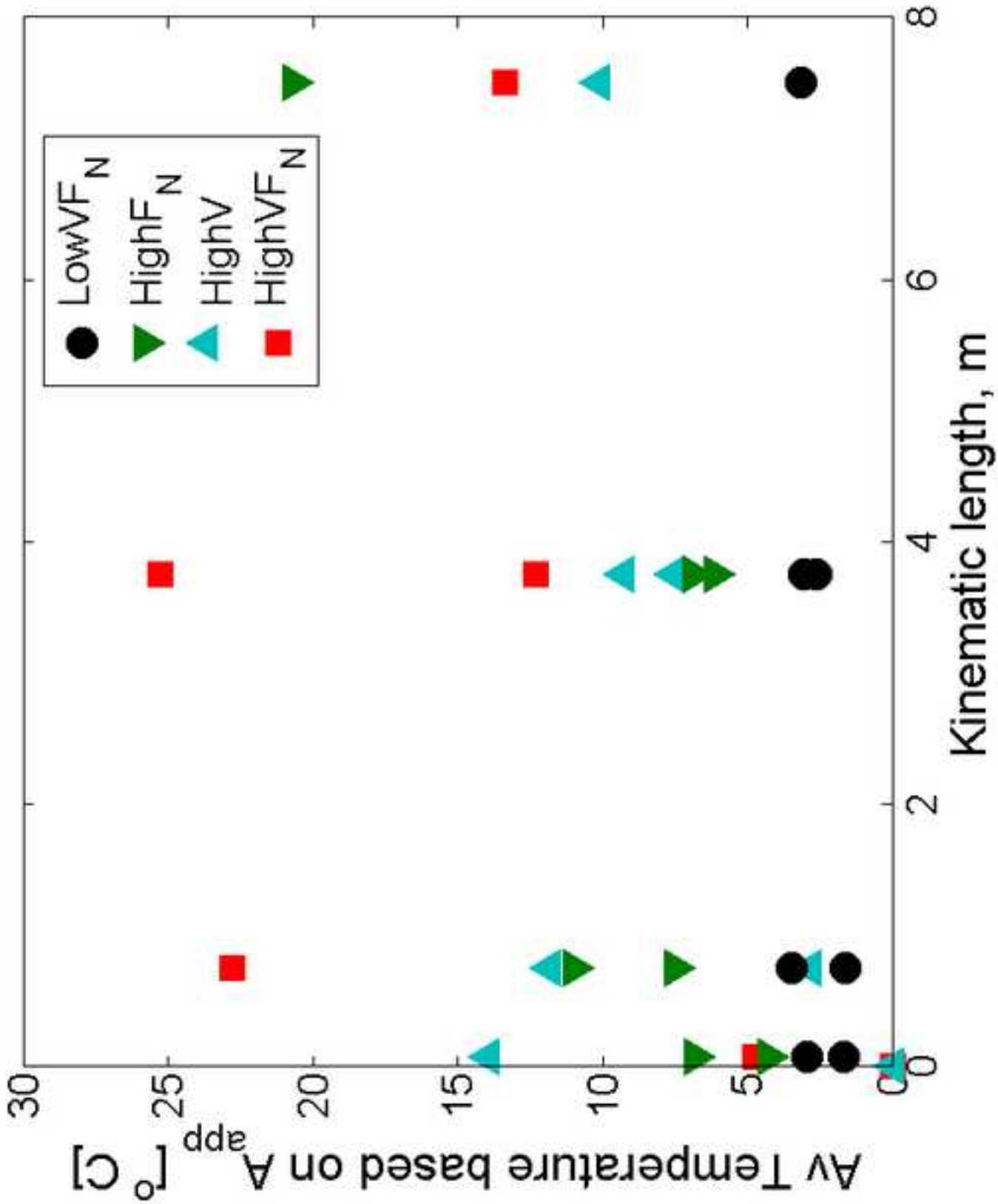
LowVF_N
HighF_N
HighV
HighVF_N
Δv Temperature based on Δ_app [° C]
Kinematic length, m
0
5
10
15
20
25
30
0
2
4
6
8

Figure(s)

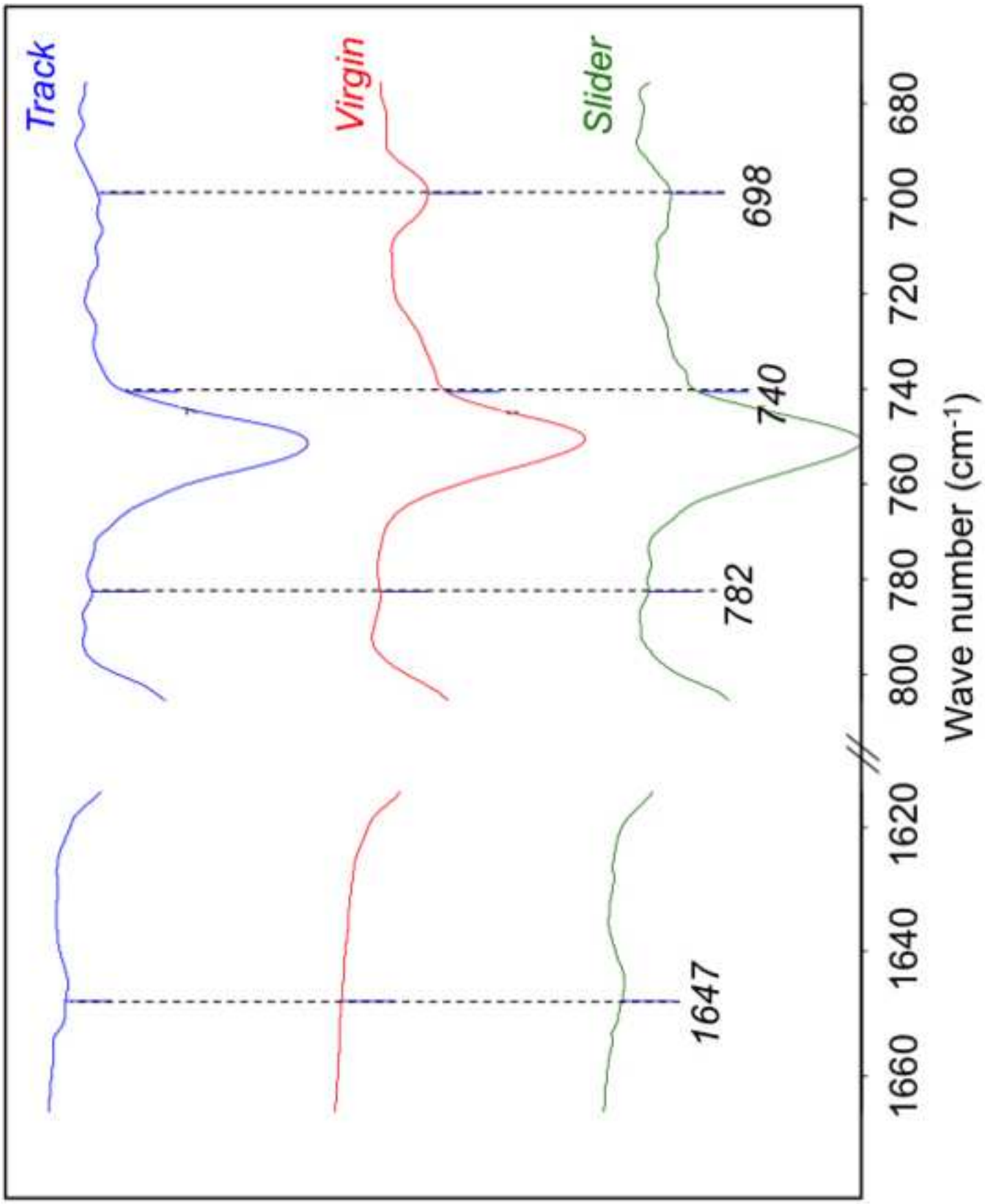
Track
Virgin
Slider
698
740
782
1647
1660
1640
1620
800
780
760
740
720
700
680
Wave number (cm-1)
Intensity (u.a.)

Figure(s)

Figure(s)